(2)

NAVAL POSTGRADUATE SCHOOL
Monterey, California

THESIS

DEVELOPMENT AND CALIBRATION OF
TWO AND FOUR WIRE WATER SURFACE WAVE
HEIGHT MEASUREMENT SYSTEMS

by

Robert Kerry Yarber

December 1992

Thesis Advisor: Robert M. Keolian
Co-Advisor: Steven L. Garrett

Approved for public release; distribution is unlimited.

Unclassified
SECURITY CLASSIFICATION OF THIS PAGE

REPORT DOCUMENTATION PAGE

Form Approved
OMB No. 0704-0188

1a. REPORT SECURITY CLASSIFICATION: UNCLASSIFIED

1b. RESTRICTIVE MARKINGS:

2a. SECURITY CLASSIFICATION AUTHORITY:

2b. DECLASSIFICATION / DOWNGRADING SCHEDULE:

3. DISTRIBUTION / AVAILABILITY OF REPORT: Approved for public release; distribution unlimited

4. PERFORMING ORGANIZATION REPORT NUMBER(S):

5. MONITORING ORGANIZATION REPORT NUMBER(S):

6a. NAME OF PERFORMING ORGANIZATION: Naval Postgraduate School

6b. OFFICE SYMBOL (If applicable): PH

7a. NAME OF MONITORING ORGANIZATION: Naval Postgraduate School

6c. ADDRESS (City, State, and ZIP Code): Monterey, CA 93943-5000

7b. ADDRESS (City, State, and ZIP Code): Monterey, CA 93943-5000

8a. NAME OF FUNDING / SPONSORING ORGANIZATION:

8b. OFFICE SYMBOL (If applicable):

9. PROCUREMENT INSTRUMENT IDENTIFICATION NUMBER:

8c. ADDRESS (City, State, and ZIP Code):

10. SOURCE OF FUNDING NUMBERS

PROGRAM ELEMENT NO.	PROJECT NO.	TASK NO.	WORK UNIT ACCESSION NO.

11. TITLE (Include Security Classification) DEVELOPMENT AND CALIBRATION OF TWO AND FOUR WIRE WATER SURFACE WAVE HEIGHT MEASUREMENT SYSTEMS

12. PERSONAL AUTHOR(S): Yarber, Robert K.

13a. TYPE OF REPORT: Master's Thesis

13b. TIME COVERED: FROM ______ TO ______

14. DATE OF REPORT (Year, Month, Day): December 1992

15. PAGE COUNT: 133

16. SUPPLEMENTARY NOTATION The views expressed in this thesis are those of the author and do not reflect the official policy or position of the Department of Defense or the U.S. Government

17. COSATI CODES

FIELD	GROUP	SUB-GROUP

18. SUBJECT TERMS (Continue on reverse if necessary and identify by block number) calibration, capacitance, conductance, four wire, gravity wave, power spectrum, surface wave height, two wire, wind-wave

19. ABSTRACT (Continue on reverse if necessary and identify by block number)

Capacitance and conductance measurements using two and four wire techniques were developed and statically and dynamically calibrated in this thesis. The voltage sensitivities range from 7.3 to 8.1 ± 0.1 mV/cm for the two wire capacitance system static calibrations. This is ± 5.2% of the limiting theoretical value. The voltage sensitivities range from 0.3 to 0.4 ± 0.1 V/cm for the four wire conductance system static calibrations. Dynamic calibrations were only completed for the conductance system. The dynamic calibration results were weakly frequency dependent with a $\omega^{-0.15}$ decay in a limited, 2-4 Hz range.

Wind power spectrum measurements were taken in the existing Upper Ocean Simulations Facility at the Naval Postgraduate School. There was excellent agreement in the spectra with both techniques.

Driven gravity wave frequency downshifting and wind energy dumping was observed in the combined gravity wave and wind-wave measurements. The power spectra peaked near two

20. DISTRIBUTION / AVAILABILITY OF ABSTRACT: ☒ UNCLASSIFIED/UNLIMITED ☐ SAME AS RPT ☐ DTIC USERS

21. ABSTRACT SECURITY CLASSIFICATION: Unclassified

22a. NAME OF RESPONSIBLE INDIVIDUAL: Robert M. Keolian

22b. TELEPHONE (Include Area Code): (408) 646-2232

22c. OFFICE SYMBOL: PH-Kn

DD Form 1473, JUN 86 Previous editions are obsolete.

S/N 0102-LF-014-6603

SECURITY CLASSIFICATION OF THIS PAGE
Unclassified

19 ABSTRACT (Continued) Hertz and decayed at 50 to 70 dB per decade, or as ω^{-5} to ω^{-7} for both systems.

Gravity wave phase speed and wavelength measurements were performed with capacitance system. The results were approximately 40% higher than theory.

Approved for public release; distribution is unlimited.

DTIC QUALITY INSPECTED 3

DEVELOPMENT AND CALIBRATION OF TWO AND FOUR WIRE WATER SURFACE WAVE HEIGHT MEASUREMENT SYSTEMS

by

Robert Kerry Yarber

B.S., Naval Postgraduate School, 1988

Accesion For		
NTIS CRA&I		X
DTIC TAB		☐
Unannounced		☐
Justification		
By		
Distribution /		
Availability Codes		
Dist	Avail and / or Special	
A-1		

Submitted in partial fulfillment of the requirements for the degree of

MASTERS OF SCIENCE IN ENGINEERING ACOUSTICS

from the

NAVAL POSTGRADUATE SCHOOL

December 1992

Author: Robert Kerry Yarber

Robert Kerry Yarber

Approved By: Robert Keolian

Robert M. Keolian, Thesis Advisor

Steven L. Garrett, Co-Advisor

Anthony A. Atchley, Chairman

Engineering Acoustics Academic Committee

ABSTRACT

Capacitance and conductance measurements using two and four wire techniques were developed and statically and dynamically calibrated in this thesis. The voltage sensitivities range from 7.3 to 8.1 ± 0.1 mV/cm for the two wire capacitance system static calibrations. This is ± 5.2% of the limiting theoretical value. The voltage sensitivities range from 0.3 to 0.4 ± 0.1 V/cm for the four wire conductance system static calibrations. Dynamic calibrations were only completed for the conductance system. The dynamic calibration results were weakly frequency dependent with a $\omega^{-0.15}$ decay in a limited, 2-4 Hz range.

Wind power spectrum measurements were taken in the existing Upper Ocean Simulations Facility at the Naval Postgraduate School. There was excellent agreement in the spectra with both techniques.

Driven gravity wave frequency downshifting and wind energy dumping was observed in the combined gravity wave and wind-wave measurements. The power spectra peaked near two Hertz and decayed at 50 to 70 dB per decade, or as ω^{-5} to ω^{-7} for both systems.

Gravity wave phase speed and wavelength measurements were performed with the capacitance system. The results were approximately 40% higher than theory.

TABLE OF CONTENTS

LIST OF TABLES

LIST OF FIGURES

LIST OF SYMBOLS

Symbol	Definition [units]
a	radius of inner charged surface [m]
$\mathbf{a}$	acceleration [m/sec^2]
A	amplitude [m]
A_o	initial amplitude [m]
b	radius of outer charged surface [m]
b	intercept of a line
B	susceptance [Seimens]
c	phase speed [m/sec]
C	capacitance [farad]
cm	centimeter
Co.	company
CCW	counter-clockwise
d	distance [m] or depth [feet]
dB	decibel
DUT	device under test
e	exponential
E	mechanical energy [joule]
F	fan
$\mathbf{F}$	force [Newton]
$F^{-1}[\,]$	inverse Fourier Transform
g/$\mathbf{g}$	acceleration of gravity [m/sec^2]
G	conductance
$G_{xy}(f)$	cross power spectral density
H	depth of fluid [m]
H_{cur}	high current terminal
H_{pot}	high potential terminal
HP	Hewlett-Packard Company
Hz	Hertz
i	current [Amp]
ID	inner diameter [m]
in	inch
Inc.	incorporated
k	wave number [m^{-1}]
kg	kilogram
kHz	kilohertz
KE	kinetic energy [joule]
l	length [m]
LCR	inductance, capacitance, and resistance
LF	low frequency
ln	natural logarithmic function
L_{cur}	low current terminal
L_{pot}	low potential terminal
m	mass [kg], meter, or slope of a line

MFG.	manufacturer
mil	millimeter
min	minute
ml	milliliter
mS	milliseimens
mV	millivolt
MHz	megahertz
n	summation dummy index
N	number variable
No.	number
o	output
OD	outer diameter [m]
OSC	oscillator
p	pressure [Pascal]
PCB	printed circuit board
PE	potential energy [Joule]
pF	picofarad
P.N.	part number
$P_N(\|r\| \geq r_o)$	probability that N measurements of two uncorrelated variables would give a coefficient r as large as r_o
Q	quality factor
r	correlation coefficient
r_o	initial correlation coefficient
R	resistance [Ohm]
®	registered trademark
R_m	mechanical resistance [kg/m]
RMS	root mean square
RPM	revolutions per minute
$R_{xy}(\tau)$	cross-correlation function
s/sec	second
$S_{x,y}(f)$	Fourier Transform of a power spectral density
t	time [s], thickness [inch], or dummy variable
T	period of time [sec]
™	trademark
v/V	voltage
v	particle velocity [m/sec]
w	width [feet]
X	reactance [Ohm]
x,y,z	Cartesian coordinates, inputs, or variables
y_e	measured dependent value
y_c	calculated dependent value
Z	impedance [Ohm]
β	temporal absorption coefficient [sec^{-1}]
f	natural frequency [Hertz]
ω	angular frequency [radian]
ρ	volume density [kg/m^3]
τ	decay time [sec] or time shift [sec]

ζ	displacement of the free surface [m]
ϕ	scalar potential
λ	wavelength [m]
∞	infinity
∇	gradient
∇^2	Laplacian
τ	period or time shift [sec]
ε	permittivity [farad/meter]
ε_o	permittivity of free space [farad/meter]
K	relative dielectric constant of a material
σ_{xy}	covariance in x and y
$\sigma_{b,m,x,y}$	standard deviation in slope, intercept, or variables x and y
Σ	summation
*	complex conjugate
'	foot
"	inch

ACKNOWLEDGMENTS

I would like to thank both of my advisors, Dr. S. L. Garrett and Dr. R. M. Keolian, for their different insights into physics and what is important in a research project, and their patience in my progress in the experiment (i.e. not firing me as a student).

I may not be a great Physicist, but I have learned to take **everything** I'm told or observe with a grain of salt. This thesis has probably taken the longest of any at NPS. My efforts to mix administrative work for the department and accomplishing useful science proved that administration got the better of me.

I would like to thank Eric Moore for all the computer aided circuit design assistance he provided me. My electronics circuits would not look as professional as they do without his help.

I would also like to thank Caroline and Cindy, my daughter and wife, for letting me have the time away from them that I needed to complete this thesis. I hope that my efforts will be worthwhile Cindy. I also insist that you press me to pass the importance and pleasures of scientific research on to Caroline.

I. INTRODUCTION

A. BACKGROUND AND MOTIVATION

In the 1980's, there were tremendous advances in the theories that describe nonlinear systems in many fields of science and engineering [Ref. 1]. These nonlinear systems vary in complexity from a simple driven pendulum, to global weather systems. This thesis studies the nonlinear system of wind wave interaction on a "deep ocean" using an existing wind wave tank, Upper Ocean Simulations Facility at the Naval Postgraduate School (NPS).

A theory describing the power spectrum of ocean surface wave crests, independent of the fetch (the distance over which wind blows over water) and duration of the generating wind, was developed by Phillips [Ref. 2]. The Phillips spectrum, based on dimensional analysis, shows a ω^{-5} spectrum for large angular frequencies, ω.

Zakharov and Filonenko later described the stochastic oscillations of the surface of a liquid with a ω^{-4} power law spectrum [Ref. 3]. In the late 1980's, Larraza applied a ω^{-4} power law spectrum to wind waves, flicker noise, solar wind, and classical second sound [Ref. 4].

There is a thirty year history of reported field and tank wind wave and driven gravity wave spectrum measurements, summarized nicely by Donelan, et. al [Ref. 5].

When Dr. Larraza came to the Naval Postgraduate School, we had an opportunity for experimentalist and theorist to collaborate in the laboratory while exploring his recent power law spectrum and second sound theories in a controlled environment.

There is also a history of laboratory controlled, in wind wave tanks, wind driven phase speed measurements. Some recent experiments which have been done to understand this phenomenon has been either flawed [Ref. 6] by aliasing due to excessive spacing of probes or were not designed to look for the effects of a turbulent restoring force [Ref. 7, 8].

Wave turbulence are those processes in open driven systems which are dominated by a random redistribution of energy (generally due to time reversible nonlinear processes) with effectively infinite degrees of freedom [Ref. 9]. Significant theoretical progress in the study of random wave systems driven far off equilibrium has lead Larraza, Garrett, and Putterman to the startling prediction of a second surface wave mode [Ref. 10]. This "second sound" mode corresponds to propagating compressions and refractions of the surface roughness.

B. SCOPE

This is the first thesis involved in the study of nonlinear wave turbulence using the existing Upper Ocean Simulations Facility at the Naval Postgraduate School. The

primary purpose of this thesis is to develop, test, and calibrate a wave height measurement system that may be used in subsequent research efforts studying various wave turbulent effects.

There were two wave height measurement system investigated in this thesis. A two-wire capacitance system and a four-wire conductance system were independently developed and tested.

Preliminary measurements were made to verify the dispersion relation for driven deep water gravity waves [Ref. 11]

$$\omega^2 = gk, \qquad \text{Eqn. 1.1}$$

where g is the acceleration of gravity and k is the wave number, and an investigation of the wind wave power spectral density and quality factor Q of the tank were conducted to help identify any tank limitations. As it stands, the second sound theory requires a power spectrum that decays as ω^{-5}. All these measurements are designed to lead to successive experiments which may confidently measure wind wave second sound.

This thesis has four chapters which describe the various aspects of the experiment. Chapter II discusses the theories of the physical properties which will be measured, and the theories of the various measurement techniques used. Chapter

III describes the wind wave tank facility and it's capabilities, the experimental apparatus construction, development, and the various calibration techniques for both systems, and the various experimental measurement techniques used. Chapter IV will present measurement results. Finally, Chapter V will discuss the conclusions of this work, and suggest directions for future research efforts.

II. THEORY

A. INTRODUCTION

This chapter discusses theories related to gravity waves, in three broad categories. These categories are variables, measurements, and techniques. The chapter will define surface gravity waves and energy density variables and then derive surface gravity wave dispersion relationships. The theories for cylindrical capacitance and four wire measurements will then be discussed. Finally, least squares fit and deviation data reduction techniques, Hewlett-Packard (HP) cross correlation measurement techniques, phase speed measurement, wavelength, and quality factor measurement techniques will be discussed.

B. SURFACE GRAVITY WAVE AND ENERGY DENSITY VARIABLES AND DISPERSION RELATIONS

> The free surface of a liquid in equilibrium in a gravitational field is a plane. If, under the action of some external perturbation, the surface is moved from its equilibrium position at some point, motion will occur in the liquid. This motion will be propagated over the whole surface in the form of waves, which are called *gravity waves*, since they are due to the action of the gravitational field. Gravity waves appear mainly on the surface of the liquid; they affect the interior also, but less and less at greater and greater depths. [Ref. 12]

A reciprocal relation between a deep water surface gravity wave phase speed and frequency will be derived in this section. Deep water is defined as a semi-infinite fluid

below a free surface. The fluid depth H is much greater than the reduced wavelength $\frac{\lambda}{2\pi}$. An intuitive feel for the surface gravity wave dispersion relation was developed by Sir M. J. Lighthill, using simple energy arguments (Rayleigh's method)[Ref. 13]. A more rigorous derivation using invisid equations for incompressible flow in a constant gravitational field can be found in "Fluid Mechanics" by L. D. Landau and E. M. Lifshitz [Ref. 14]. Both developments will be presented here.

1. Rayleigh's Method

The gravitational potential energy PE per unit horizontal area, at any point on the surface, is found by integrating the potential energy per unit volume from the surface to the bottom. The maximum excess potential energy per unit horizontal area over the displacement of the undisturbed free surface ($\zeta = 0$) is

$$PE = \frac{1}{2}\rho g \zeta^2,$$

Eqn. 2.1

where ρ is the volume density of the liquid.

The kinetic energy KE per unit horizontal area of a sinusoidal wave is

$$KE = \frac{1}{2}\rho k^{-1}\left(\frac{\delta\zeta}{\delta t}\right)^2,$$

Eqn. 2.2

where t is the time

The mechanical energy E per unit area of the system is E = KE + PE. The deep water surface gravity wave dispersion relation is found by setting the maximum value of equation (2.1) equal to the maximum value of equation (2.2),

$$\omega^2 = gk,$$

Eqn. 1.1

which can be further reduced using phase speed c, $c = \omega/k$, and the relationship between angular frequency and natural frequency, $\omega = 2\pi f$, to

$$c = \frac{g}{2\pi f}.$$

Eqn. 2.3

The above simple result assumed that there was an exponential decay of velocity away from the surface which restricts equation (1.1) to deep water.

2. Invisid Equations

The derivation using invisid fluid equations begins with Newton's Second Law, $\mathbf{F} = m\mathbf{a}$. Bold letters represent vectors. The equation of motion of a fluid is determined if this force is equated to the gradient of the pressure p on a unit volume, $\mathbf{F} = m\mathbf{a} = \nabla p$. The equation of motion of a fluid

was developed by L. Euler in 1778 [Ref. 15]. Euler's equation in a gravitational field is given by

$$\frac{\delta \mathbf{v}}{\delta t} + (\mathbf{v} \cdot \nabla)\mathbf{v} = -\frac{\nabla p}{\rho} + \mathbf{g}.$$

Eqn. 2.4

where $\mathbf{v}$ is the particle velocity.

Fluid particles in a gravity wave travel on the order of the amplitude A of the wave during a time interval of period T. The particle velocity is of the order A/T. The velocity varies noticeably over time intervals of the order T and distances of the order of the wavelength λ in the direction of propagation. The time derivative of the velocity $\frac{\delta \mathbf{v}}{\delta t}$ is of the order v/T, and the space derivative $\nabla \mathbf{v}$ is of the order $\mathbf{v}/\lambda$. The left side of equation (2.4) is approximately equivalent therefore to

$$\frac{\delta \mathbf{v}}{\delta t} + (\mathbf{v} \cdot \nabla)\mathbf{v} \approx \frac{A}{T}\frac{1}{T} + \frac{1}{\lambda}\left(\frac{A}{T}\right)^2$$

Eqn. 2.5

We can neglect the $(\mathbf{v} \cdot \nabla)\mathbf{v}$ term if the amplitude of the oscillations in the gravity wave are small compared with the wavelength, A << λ, and we have potential flow.

The equation of continuity in a potential flow of an incompressional fluid is

$$\nabla^2 \phi = 0,$$

Eqn. 2.6

i.e. Laplace's equation for scalar potential ϕ, $\mathbf{v} = \nabla\phi$. Integrating equation (2.4) after neglecting the $(\mathbf{v}\cdot\nabla)\mathbf{v}$ term and a little algebraic manipulation, gives

$$p = -\rho \mathbf{g} z - \rho \frac{\delta\phi}{\delta t}.$$

Eqn. 2.7

Let $\zeta = \zeta(x,y,t)$ be the z coordinate of a point on the surface. If a constant pressure p_o acts on the surface, equation (2.7) reduces to

$$0 = \mathbf{g}\zeta + \left.\frac{\delta\phi}{\delta t}\right|_{z=\zeta}.$$

Eqn. 2.8

The z coordinate of a point on the surface is now

$$\zeta = -\frac{1}{\mathbf{g}} \left.\frac{\delta\phi}{\delta t}\right|_{z=\zeta}.$$

Eqn. 2.9

The vertical component of the velocity of a point on the surface is

$$\mathbf{v}_z = \frac{\delta\zeta}{\delta t},$$

Eqn. 2.10

but $\mathbf{v}_z = \frac{\delta\phi}{\delta z}$, so that

$$\left(\frac{\delta\phi}{\delta z}\right)_{z=\zeta} = \frac{\delta\zeta}{\delta t}.$$

Eqn. 2.11

Substituting equation 2.9 into 2.11 we obtain

$$\left(\frac{\delta\phi}{\delta z} + \frac{1}{g}\frac{\delta^2\phi}{\delta t^2}\right)_{z=\zeta} = 0.$$

Eqn. 2.12

The system of equations which determine the motion in a gravitational field are:

$$\nabla^2\phi = 0,$$

Eqn. 2.6

$$\left(\frac{\delta\phi}{\delta z} + \frac{1}{g}\frac{\delta^2\phi}{\delta t^2}\right)_{z=\zeta} = 0.$$

Eqn. 2.12

Assume that the velocity decays exponentially away from the surface at a rate k. The velocity potential of the deep water surface gravity wave propagating in the x-direction and uniform in the y-direction is,

$$\phi = A_o e^{kz}\cos(kx-\omega t).$$

Eqn. 2.13

Substituting equation 2.13 into the boundary conditions of equation 2.12, we obtain

$$k - \frac{\omega^2}{g} = 0$$

Eqn. 2.14

or

$$\omega^2 = gk.$$

Eqn. 1.1

This gives the same deep water surface gravity wave dispersion relation between wave number and angular frequency, as developed using Rayleigh's method.

The deep water approximation will start breaking down when the bottom of the tank interferes with the solution given by equation (2.13). This will occur if the e^{kz} term is non-negligible at $z = -H$, H being the depth of the water, which occurs when $k \leq \frac{1}{H}$. For our tank, H = 1m so the deep water approximation is good for $\lambda >> \frac{2\pi}{k} = 2\pi H = 6.3$ m and $f >> \frac{1}{2\pi}\sqrt{\frac{g}{H}} = 0.20$ Hz.

C. TRANSDUCER PRINCIPLES

Understanding the electrical properties that are proportional to changes in surface water height are an essential part of this thesis. The electrical properties and measurement techniques used in this work will be discussed next.

In an electrical circuit, complex electrical impedance is proportional to voltage changes when a constant current is applied to the circuit. The first type of transducer described in this thesis is based on applying a constant voltage and measuring the change of capacitance with respect

to the length of a cylindrical capacitor as a function of water height.

The second type of transducer described in this thesis is based on applying a constant current and measuring the change in the magnitude of the complex impedance with respect to an effective cross sectional area of a volume of water under test. The impedance is inversely proportional to the water height.

This section will detail both transduction properties and the associated measurement techniques.

1. Cylindrical Capacitance

A vertical insulated wire penetrates the surface of water approximately forming a cylindrical coaxial capacitor. The wire is the inner conductor, the insulation is the dielectric, and the water bath acts as an outer conductor of changing length.

To ensure that our system is behaving as expected, the theoretical limiting capacitance of an ideal cylindrical conductor must be compared to the measured capacitance of the cylindrical probe wires. The capacitance of an ideal cylindrical conductor is given by [Ref. 16]

$$C = \frac{2\pi\varepsilon}{\ln\left(\frac{b}{a}\right)}\, l, \qquad \text{Eqn. 2.17}$$

where

ε is the permittivity, $\varepsilon = K\varepsilon_o$;

K is the relative dielectric constant of a material;

ε_o is the permittivity of free space;

l is the length of the conductor, proportional to the height of the water;

ln is the natural logarithmic function;

b is the radius of the outer charged surface; and

a is the radius of the inner charged surface.

The permittivity of free space is $\varepsilon_o = 8.854 \times 10^{-12}$ farad/meter.

The resistivity of the water in our tank is surprisingly low. A few inches of 0.2 mm diameter wire has a resistance to infinity of only 20 ohms. The capacitive impedance of our probe is many times higher, so that the water can be taken to be a perfect conductor. Electrical contact to the water is made in a two-wire measurement configuration through a second submerged wire at "infinity", many probe wire diameters away.

A measurement of the capacitance gives the height, with the theoretical sensitivity $\frac{\delta C}{\delta l}$ for the final capacitive test probes given by $\frac{2\pi\varepsilon}{\ln\left(\frac{b}{a}\right)} = 56.1$ pF/m.

The two-wire capacitive scheme suffers from an unknown, unsteady, artifactual complex impedance between the probe and the bath at the very small length scales of the

order of a probe diameter. For example, the water meniscus slips and sticks to the probe because of a surface film that collects on the probes, instead of sliding freely as the water height oscillates. This film can itself add an unknown series resistance. And it is also possible that the conductivity of the water in the immediate vicinity of the probes is changing because of poorly understood electrochemistry at the metal-water-ion interface. For these reasons, we developed a four wire probe, based on the four wire impedance measuring technique commonly used in electronics and solid state physics.

2. Measurement Technique Models

The physical electrical connections between an analyzer and a device under test (DUT), water in our case, using a two-wire measurement technique can be modeled as unknown variable resistors in an equivalent electrical circuit as shown in Figure (2.1). A constant current i is measured and applied to the DUT and the voltage v is measured across the series combination of the unknown lead impedance and the DUT impedance.

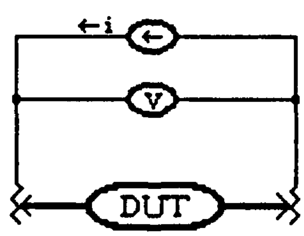

Figure 2.1. Two wire measurement equivalent circuit.

Four wire, or four terminal pair configuration, measurements provide significant measuring advantage over a two wire measurement, for some situations. The HP-4192A and HP-4194A Impedance Analyzers are designed to make four wire measurements. The combination of equipment and measurement technique provides an accurate and easy measurement.

A four wire measurement uses four connectors: High Current (H_{cur}), High Potential (H_{pot}), Low Potential (L_{pot}), and Low Current (L_{cur}) [Ref. 17]. The unknown variable impedances of the potential leads, as shown in the equivalent electrical circuit in Figure (2.2), are unimportant because there is no current in that portion of the circuit due to the high, nearly infinite, impedance of the voltmeter. Likewise, the unknown impedance of the current leads are unimportant because the current flowing through them is known, and all this current flows through the DUT.

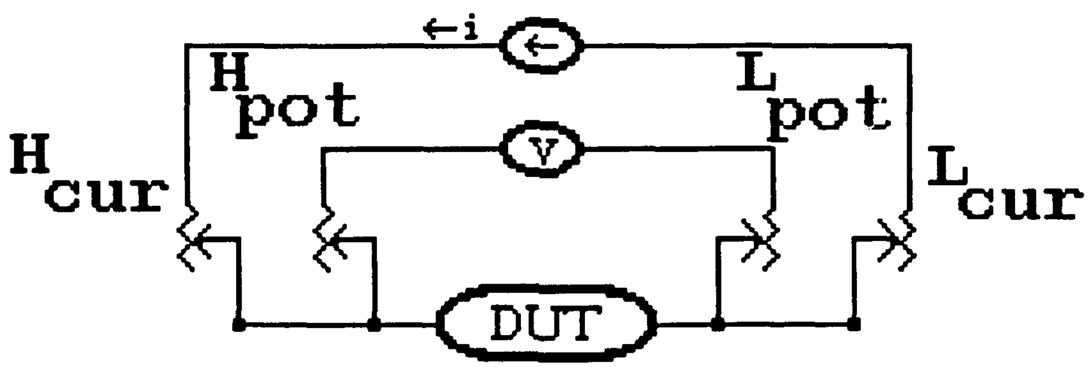

Figure 2.2. Four wire measurement equivalent circuit.

3. Four-Wire Conductance Technique

Conductance is inversely proportional to the magnitude of the complex impedance. Conductance is proportional to changes in the water height. The conductance is obtained using the four-wire measurement technique by inverting the voltage difference in the water when measuring the complex impedance.

The complex impedance Z of a device under test DUT is given by

$$Z = \frac{\rho l}{h\ W_{eff}} = \frac{\Delta V}{i}$$

Eqn. 2.16

where

ρ is the complex resistivity of the conductor (water in our case);

l is the length of the conductor, proportional to the separation between the potential leads in the water;

h is the height of the conductor on the wires;

W_{eff} is the effective width of the conduction path between the wires;

$\Delta V = H_{pot} - L_{pot}$;

i is the current applied to the circuit.

Figure (2.3) illustrates a four-wire resistance measurement in water.

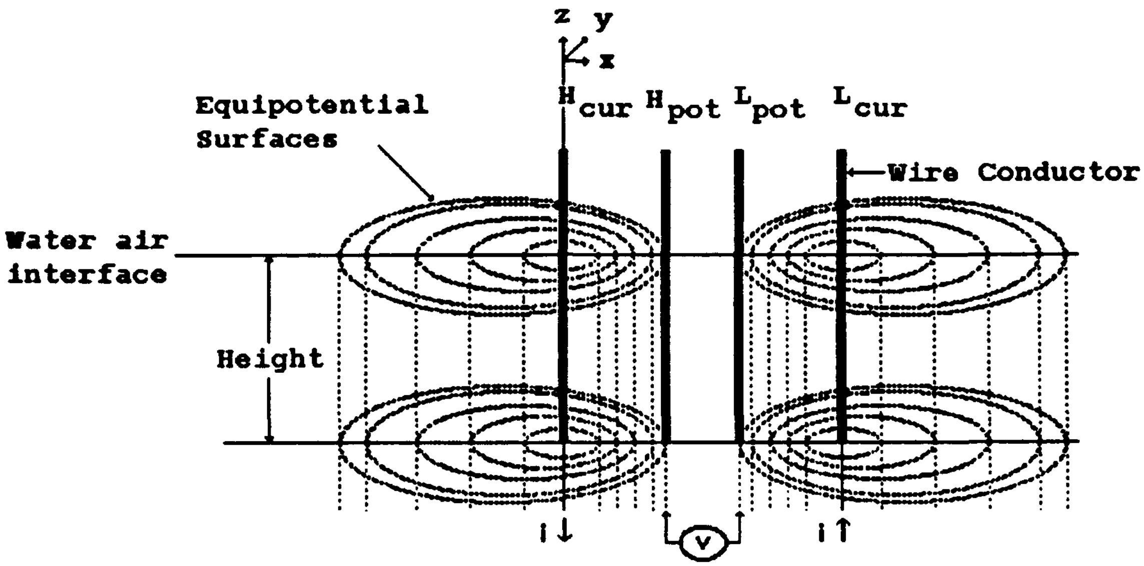

Figure 2.3. Four-wire resistance measurement.

Because it is based on the four-wire technique, our probe is insensitive to possible conductance changes of the water or to other contact impedances between the wire and the water on the "micro scale" illustrated in Figure (2.4). However, the four wire technique would be sensitive to changes in conductance on the "macro scale" between the probe wires. We do not know if this is a problem, or not.

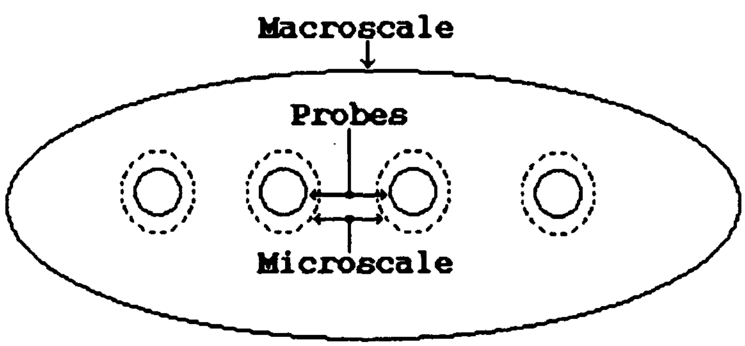

Figure 2.4. Macro/micro scales about a four-wire sensor.

D. LEAST SQUARES FIT AND DEVIATION ANALYSIS TECHNIQUES

The method of least squares for fitting data to a straight line can be accomplished on most hand-held scientific calculators today. The calculator automatically accumulates the necessary sums to provide slope, intercept, and linear correlation coefficient. Unfortunately, the correlation coefficient is not directly related to the uncertainty in the least squares values of the slope and intercept, which are the quantities of interest. [For a full development of the method of least squares fit, see reference 18].

The correlation coefficient r indicates whether there is causal relationship between the variables x and y, and therefore whether a linear fit to the data is justified. The correlation coefficient is defined by Taylor [Ref. 19] in terms of the covariance, σ_{xy}, and standard deviations σ_x and σ_y. A more intuitive picture of the correlation can be developed by determining the slope m of a line of the data set when it is plotted y vs. x, and then when it is plotted x vs. y (which we will call m'). If there were no errors in the measurements and the measurement x and y obey a linear relation, then these two slopes would be a negative inverse of one another (i.e. $m = -1/m'$) and $r^2 = 1$, where r is defined as $r = \frac{m}{|m'|}$. If there is noise in the data, then $r^2 < 1$.

The quantitative significance of r is found when r is expressed in terms of probability. For any defined r_o, $P_N(|r|\geq r_o)$ is the probability that N measurements of two uncorrelated variabl^s would give a coefficient r as large as r_o. The probability that N measurements were derived from a random process involves the integration of a two dimensional Gaussian distribution [Ref. 20]. Generally it is more convenient to use a table which contains a value for r which would have to be exceeded for there to be a probability less than $P_N(|r|\geq r_o)$ that the N measurements were generated by a random sample of observations taken from uncorrelated parent population. Two such tables are included in Taylor [Ref. 21].

For physical measurements, it is the error in the least square values of the slope and intercept which are of interest. Taylor gives expressions for the standard deviation in y, σ_y, error in the slope, σ_m, and intercept, σ_b, in terms of the accumulated sums which are available in memory of most scientific calculators. I have reproduced them below:

$$\sigma y = \sqrt{\frac{\sum_{n=1}^{N}(\delta y_n)^2}{N-2}},$$

Eqn. 2.16

$$\sum_{n=1}^{N}(\delta y_n)^2 = \Sigma y_n^2 - \frac{(\Sigma y_n)^2\Sigma x_n^2 - 2\Sigma(x_n y_n)\Sigma x_n \Sigma y_n + N[\Sigma(x_n y_n)]^2}{N\Sigma x_n^2 - (\Sigma x_n)^2},$$

Eqn. 2.17

$$\sigma_b = \sigma_y \sqrt{\frac{\Sigma x_n^2}{N\Sigma x_n^2 - (\Sigma x_n)^2}},$$

Eqn. 2.18

$$\sigma_m = \sigma_y \sqrt{\frac{N}{N\Sigma x_n^2 - (\Sigma x_n)^2}},$$

Eqn. 2.19

where n is a summation dummy index.

Data sets were analyzed and errors in the fit parameters were determined using this technique throughout the thesis. Program code to determine the standard deviations in intercept, slope, and y using a HP-15C calculator is documented in Appendix A. The data was also analyzed using a Microsoft™ Excel file using equations (2.16) through (2.19).

It is also important to determine if there are random or systematic errors when examining experimental measurements. Random errors are revealed by repeating the measurements. Systematic errors cannot be revealed this way. Deviations in the least-square fit data are computed by subtracting the

regression calculated dependent value y_c, from the measured dependent value y_e [Ref. 22],

$$\text{Deviation} = y_e - y_c.$$

Eqn. 2.20

Plotting the deviations helps reveal what type of errors are showing up in the measurement data.

E. HEWLETT-PACKARD ANALYZER CROSS CORRELATION MEASUREMENTS

"Correlation is a measure of similarity between two quantities" [Ref. 23]. This measurement technique allows you to measure a very small signal in the presence of noise. The dynamic signal analyzer can make this type of measurement well for very low frequency or single shot measurements, and provides a signal output in the time domain.

There are two types of correlations: the auto-correlation function and the cross-correlation function. The results of the different correlations can be the same; however, the different correlations are applied to different types of systems. The auto-correlation function is a single channel measurement and the cross-correlation function is a two-channel measurement.

The cross-correlation function compares two different signals as a function of the time shift between them [Ref. 24], and is given by

$$R_{xy}(\tau) = \lim_{T\to\infty} \frac{1}{T} \int_0^T x(t)y(t+\tau)dt$$

Eqn. 2.21

where x is one input, y is another input, ∞ is infinity, and τ is the time shift between the inputs.

When the same signal is present in both channels in the presence of noise, the noise can be greatly removed using this technique. The correlation analysis is made when the dynamic signal analyzer is making a power spectral density measurement.

Power spectral density measurements are made by the dynamic signal analyzer for each channel. A cross power spectral density is then computed internally, which is the product of the Fourier Transform of the two signals [Ref. 25], and is given by

$$G_{xy}(f) = S_x(f) S_y^*(f)$$

Eqn. 2.22

where f is the natural frequency and * indicates the complex conjugate of the function.

The HP cross-correlation is then computed indirectly using the cross power spectrum [Ref. 24], and is defined as

$$R_{xy}(\tau) = F^{-1}[G_{xy}(f)].$$

Eqn. 2.23

F. GRAVITY WAVE PHASE SPEED AND WAVELENGTH MEASUREMENTS

The phase speed of a sinusoidally driven gravity wave can be measured in a two-point measurement system using the output of the signal analyzer cross-correlation function and the distance between the sensor probes. This technique was used as a check of the capacitance probes.

The phase speed of a wave is given by

$$c = f\lambda,$$

Eqn 2.24

and the theory of deep water gravity waves gives this speed as

$$c = \frac{g}{2\pi f}.$$

Eqn. 2.3

Experimentally, the phase speed of a wave in the x-direction can be determined from the period of time T that a particular phase of the wave, such as a crest or trough, takes to move a given distance d. The phase speed is given by

$$c = \frac{d}{T}$$

Eqn. 2.25

where the distance d is the distance between the probes.

The cross-correlation output of a sinusoidal signal will also be a sinusoid, in the time domain. The period of a full or half cycle of a driven surface gravity wave can be determined from the cross-correlation measurement output. The period is determined using the method of least squares fit to the measured cross-correlation minimum or maximum data points.

The phase speed is then a simple computation using equation (2.25). The driven surface gravity wave wavelength is determined using the measured period and computed phase speed. The natural frequency is the inverse of period, i.e. $f = \frac{1}{T}$. Substitute this into equation (2.24) and solve for wavelength to get

$$\lambda = cT.$$

Eqn. 2.26

G. FREE DECAY QUALITY FACTOR, Q MEASUREMENT

The amplitude of a damped oscillator decreases exponentially with time. The amplitude may be represented by

$$A(t) = A_o e^{-\beta t},$$

Eqn. 2.27

where A_o is the initial amplitude and β is called the temporal absorption coefficient. The length of time for a

damped oscillator to decay to 1/e of the initial amplitude, is called the decay time τ, defined by

$$\tau = \frac{1}{\beta} = \frac{2m}{R_m},$$

Eqn. 2.28

where m is the mass and R_m is the mechanical resistance [Ref. 26].

Substitute equation (2.28) into equation (2.27) and take the natural logarithm of the equation to get

$$\ln [A(t)] = \ln [A_o] - \frac{1}{\tau} t.$$

Eqn. 2.29

Using a change of variables, letting $y = \ln [A(t)]$, $m = -\frac{1}{\tau}$, and $b = \ln [A_o]$ we get the equation of a line,

$$y = mt + b.$$

Eqn. 2.30

For a continuous frequency system, such as the spectrum of a wind wave tank, the amplitude vs. time can be measured. Plotting ln [A(t)] verses time, b and m can be determined using the method of least squares fit. The decay time can then be computed for any frequency f_o by

$$\tau = -\frac{1}{m}.$$

Eqn. 2.31

Another method of reporting this decay is in terms of the quality factor, or "Q of the system". The quality factor of a damped oscillator is defined [Ref. 27],

$$Q = \frac{\omega_o}{\omega_2 - \omega_1}, \qquad \text{Eqn. 2.32}$$

where ω_2 and ω_1 are average half power frequencies, above and below resonance ω_o, respectively.

I will not discuss the physics of a damped oscillator. This is discussed in "*Fundamentals of Acoustics*" [Ref. 28]. The Q can be expressed in terms of the mechanical constants of the system, given by

$$Q = \frac{\omega_o m}{R_m}. \qquad \text{Eqn 2.33}$$

Substituting the decay time from equation (2.28) gives

$$Q = \frac{1}{2}\omega_o \tau, \text{ or}$$
$$Q = \pi f_o \tau. \qquad \text{Eqn. 2.34}$$

Note that Q is a dimensionless quantity.

III. EXPERIMENT

A. INTRODUCTION

The goal of our experimental program, of which this thesis is the first part, is to measure second-order (nonlinear) effects on deep water surface gravity waves. A very sensitive and linear measurement system is required so that transduction artifacts, such as non linearity, hysteresis, noise, etc., will be minimized. Interpretation of second-order effects will be much more reliable if we can ensure that we are using a linear, low noise, high sensitivity, wave height transducer system.

There were two wave height transducer systems investigated in this thesis. The two-wire capacitance system was developed and tested until it was determined that the system was unsuitable for these applications. A four-wire conductance system was then developed and tested. The transducer systems development and testing are presented in parallel.

The experimental apparatus can be divided into four major components, as shown in Figure (3.1). The first component is the wind-wave generating tank system. The tank system was originally built in the 1960's by Professor Herman Medwin for use in experiments to measure sound scattering produced by wind driven waves on rough surfaces

[Ref. 29]. It was upgraded for these experiments. The second component is the sensor. Two sensor types were tested in these experiments. The third component is the associated electronics designed and built for each sensor. The final component is the off the shelf, general laboratory instrumentation.

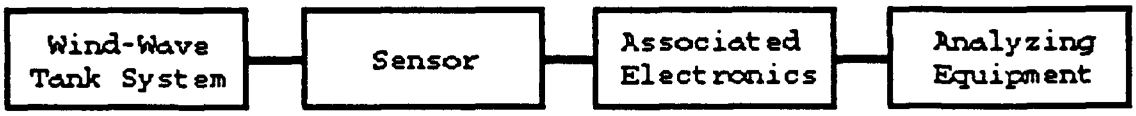

Figure 3.1. Experimental block diagram.

This chapter will describe the general calibration techniques used, some of the design criteria and detailed construction of the experimental apparatus components (i.e., sensor, associated electronics, and the wind-wave tank system), and the specific calibration of all the apparatus. Finally, the techniques and experimental procedures used for the deep water surface gravity wave measurements will be detailed.

The thesis will have several charts and tables that are referenced to the thesis lab books. The system will be lab book number, page number, represented by (B#P#).

B. WIND-WAVE TANK SYSTEM

1. Tank Facility

This section will describe the capabilities and dimensions of the existing wind-wave tank and upgrades, the

first experimental component. The wind-wave tunnel section is 57 feet long, built primarily above ground, as shown in Figure (3.2). The tunnel is constructed of 3/4 inch plywood, fiber glassed for waterproofing, with 19 (2' x 4' x 0.5")(l x w x t) plate glass view ports. The water cross section of the tunnel is (4 x 3.5 feet) (w x d). The wind cross section of the tunnel is (4 x 0.5 feet) (w x d). The depths are, of course, only approximate, since they depend on the quantity of water placed in the tank.

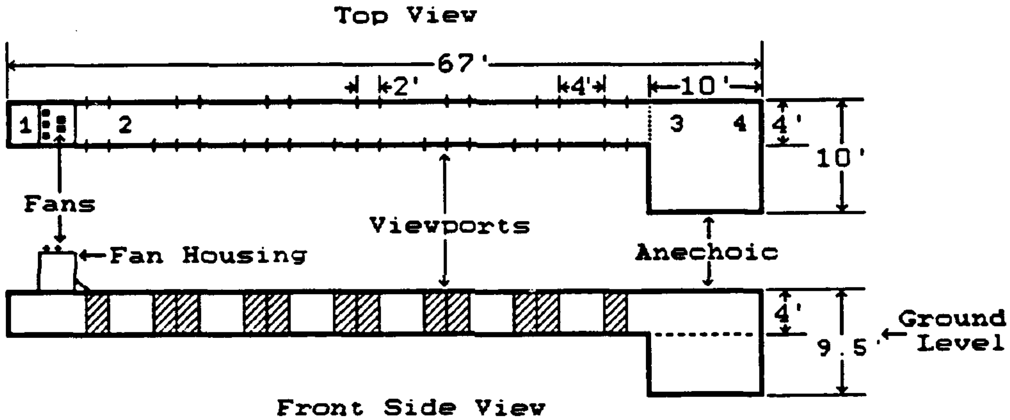

Figure 3.2. Wind-wave tank.

The anechoic section is (10 x 10 x 9.5 feet)(l x w x d) sunk into the ground, also shown in Figure (3.2). This section of the tank is constructed of six inch reinforced concrete and has (4" x 4" x 9.5')(l x w x t) redwood wedges, used on the four sides and the bottom to absorb underwater sound in previous experiments. The top of this section has two removable 3/4 inch reinforced plywood covers for personnel safety.

2. Small Wave Guide

A paddle driven at large amplitude, can generate parametric waves that run transverse to the directly driven wave. These waves interfered with the dynamic calibration of the four wire probe. You can cutoff these unwanted waves using a wave guide. A small wave guide was constructed and placed in the main tank as shown in Figure (3.3).

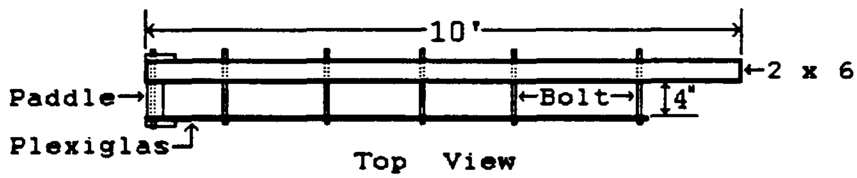

Figure 3.3. Small wave guide.

This wave guide has only two sides and a small paddle at one end. The top, bottom, and end opposite the paddle are open to the main tank. The minimum width of the wave guide was determined by the minimum width of the conductive probe, which was calibrated in this wave guide. The cutoff for this wave guide is 3.95 Hz.

One side of this wave guide is a (2" x 6" x 10')(t x w x l) pine board. The other side is a (0.060" x 2' x 8')(t x w x l) Plexiglas plate. The Plexiglas is used so that the wave structure in the wave guide can be seen. The two sides are held together with six, eight inch long, $\frac{3}{8}$-16 bolts, five, four inch Teflon spacers between the sides, and six, $\frac{3}{8}$-16 hex nuts.

A (2 x 4 x 13 inch)(t x w x l) pine board was used for the paddle. An eight inch long, $\frac{3}{8}$-16 bolt went through a half inch hole that was drilled at one end of the paddle and two ($\frac{3}{4}$ x 5.5 x 16 inch)(t x w x l) pine boards that were also bolted to the wave guide sides. A wave driver is connected to a 16 inch L-channel which was bolted to the top of the paddle.

3. Wind Generation

The wind source consist of five pairs of $\frac{3}{4}$ horsepower centrifugal fans on the top of a (39 x 48 x 41 inch) (l x w x h) housing. This housing is attached to the tunnel between locations one and two in Figure (3.2). There are three power switches for the fan bank resulting in seven combinations of powered fans.

The wind was measured approximately four feet from the wind-water interface, approximately in the center of the wind tunnel cross sectional area, at location two in Figure (3.2). Wind speed was measured using a hand held Turbo-meter™ manufactured by Davis Instruments of San Leandro, CA. The uncalibrated, measured wind speeds are reported in Table (3.1).

TABLE 3.1. WIND AND SURFACE DRAG SPEED AT LOCATION TWO (B2P55P131).

Fan Combinations	Wind Speed (m/s ± 0.1)	Surface Drag Speed (m/s ± 0.01)
F1	Too small to measure	0.09
F2	2.7	0.09
F3	2.9	0.12
F1 + F2	4.2	0.12
F1 + F3	6.5	0.19
F2 + F3	6.0	0.17
F1 + F2 + F3	7.0	0.22

4. Wave Driver

The wave driver is a gravity wave source. Three wave drivers will be described in this section.

a. Medwin Wave Driver

The Medwin wave driver was developed and used in previous experiments in the tank system. The Medwin wave driver has a fixed amplitude and four drive frequencies. It consists of a forcing wedge and belt driven electro-mechanical plunging system. New wave drivers were developed for these experiments after initial tests in the tank determined that the Medwin wave driver was nonlinear itself.

The forcing wedge was a right triangle wedge that is pushed and pulled up and down in the water, Figure (3.4). The 1716 cubic inch right triangle wedge is constructed using $\frac{3}{4}$ inch plywood sides, braced with $\frac{3}{4}$ inch plywood on both ends and in the center, and open on the top. There are one and a half inch guide strips on the outside of both ends of the wedge that are inserted into tracks built in the end of the tank just behind the fan housing. The tracks help direct the wedge movement up and down into the water. The entire wedge is treated with waterproof paint for submersion into water. Sand is uniformly placed inside the wedge to increase the weight in an attempt to increase the wedge stability.

The plunging system consist of an electric motor, a fixed mechanical speed reducer, fly wheel, and two plunging rod assemblies shown in Figure (3.5). The electric motor is a Dayton Electric MFG. CO., model number 5K452C, half horsepower, 1725 RPM, 60 Hz, single phase, capacitive start motor. The motor is mounted on standard (1 x 1.5 x 10 inch) motor mounts. The motor mounts are attached to a (11 x 8 x $\frac{3}{8}$ inch)(l x w x t) aluminum plate using four, one inch long, $\frac{3}{8}$-16 bolts. This plate is attached to a (13 x 22 x $\frac{3}{8}$ inch)(l x w x t) aluminum bottom plate using an eight inch piano hinge and a four and a half inch long, $\frac{1}{2}$-13 bolt. This construction allowed the position of the motor to be easily changed for belt adjustment and/or replacement. The large

bottom plate is shock mount to two (3.5 x 3.5 x 24.5 inch)(t x w x l) redwood boards. These boards are clamped to aluminum L-beams that span the top of the tank, just behind the fan housing at location one in Figure (3.2). The plunging system is mounted above the water directly above the wedge.

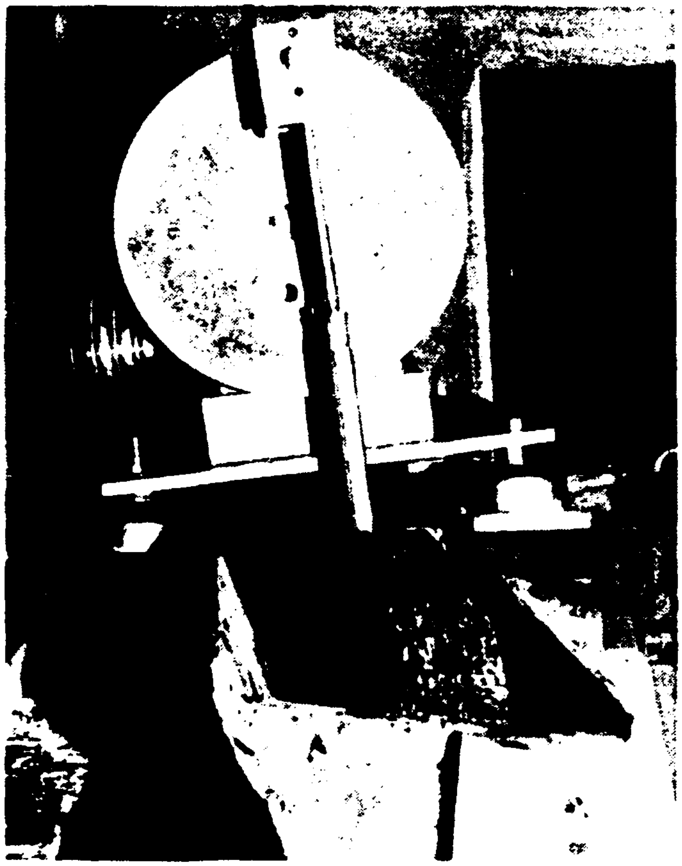

Figure 3.4. Medwin wave plunger.

The mechanical speed reducer is an Alling-Lander Co., Inc., model number CU-20, 20 to 1 ratio reducer. An aluminum ten inch diameter flywheel is attached to the $\frac{3}{4}$ inch diameter output drive axle. An eight inch long, $\frac{7}{8}$ inch diameter stainless steel rod, with two and a half inches of $\frac{1}{2}$-13 threads is connected to the output flywheel.

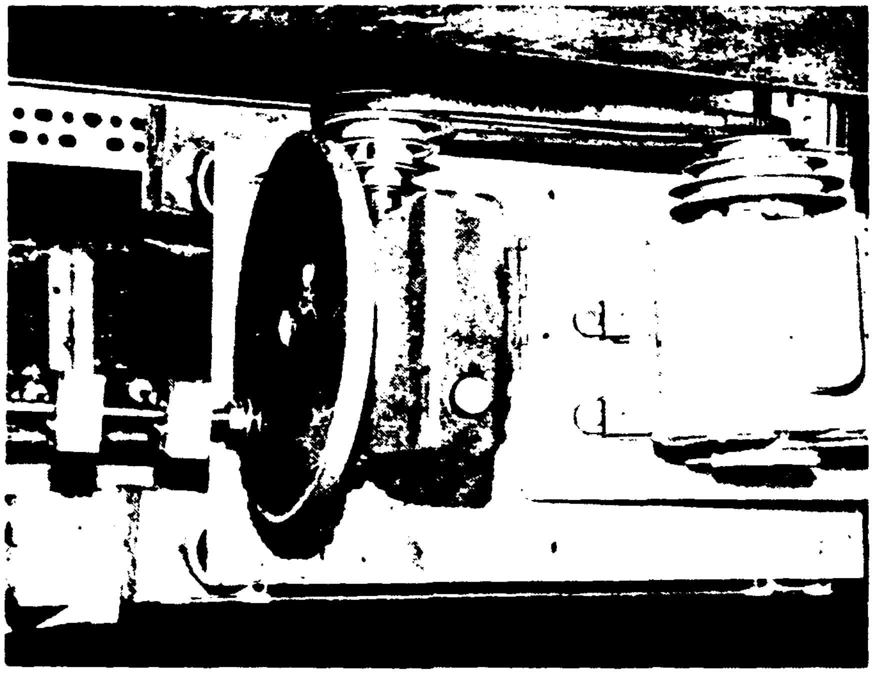

Figure 3.5. Medwin drive system.

A Craftsman™, catalog number 9-1631, ($\frac{1}{2}$ x 31 inch) engine belt is used to connect the electric motor to the mechanical speed reducer. The speed reducer is mounted to the bottom plate also. The belt is used on two, four position, flywheels. Positioning the belt in any of four flywheel combinations determined which of the four output frequencies the system generated.

The plunger rods assembly consisted of two (2 x 2.5 x 1 inch) aluminum bearing housing, which are attached to the $\frac{7}{8}$ inch diameter rod on the flywheel. The housings have a $\frac{3}{8}$-16 threaded hole that a 14.5 inch threaded rod may be screwed into and held with a lock nut at the housing. A seven inch turn buckle is attached to the other end of the

threaded rod. A two and a half inch eye bolt is attached to the other end of the turn buckle. A six inch long $\frac{3}{8}$-20 bolt with nuts goes through the eye bolt and the center pieces of plywood in the wedge, completing the plunger system.

The non linearity was not quantified, but was readily apparent when watching the erratic plunging action and resulting waves of this driver. The wedge would not move up and down in a uniform motion. It erratically got caught in the guides due to the fact that the force from the plunger rods was not always normal to the wedge itself. This caused the wedge to be pushed or pulled from side to side as well as up and down.

b. Yarber Wave Driver

The Yarber wave driver is continuously variable in both frequency and amplitude. It has a forcing paddle and a direct drive electro-mechanical plunging system.

The paddle is a (12 x 44 x $\frac{3}{4}$ inch)(w x l x t) pine board with a (15 x 4 $\frac{3}{4}$ inch) tab, which is just right of the center line as shown in Figure (3.6). The paddle is attached to two (2" x 4" x 4')(t x w x l) boards with two, three and a half inch hinges. The two by fours are clamped to the end of the wave tank, using two six inch C-clamps.

The paddle system consist of an electric motor, a direct drive speed reducer, and a single plunging rod assembly shown in Figure (3.7). The motor is a General Electric Co., model number 5KC45PG1140H, $\frac{3}{4}$ horsepower, 1725

RPM, 60 Hz, single phase, capacitive start motor. The motor is connected to a Zero-Max® direct drive, model number QX1, CCW output, zero to 400 RPM continuously variable speed mechanical reducer. Full specifications are found in Reference 30.

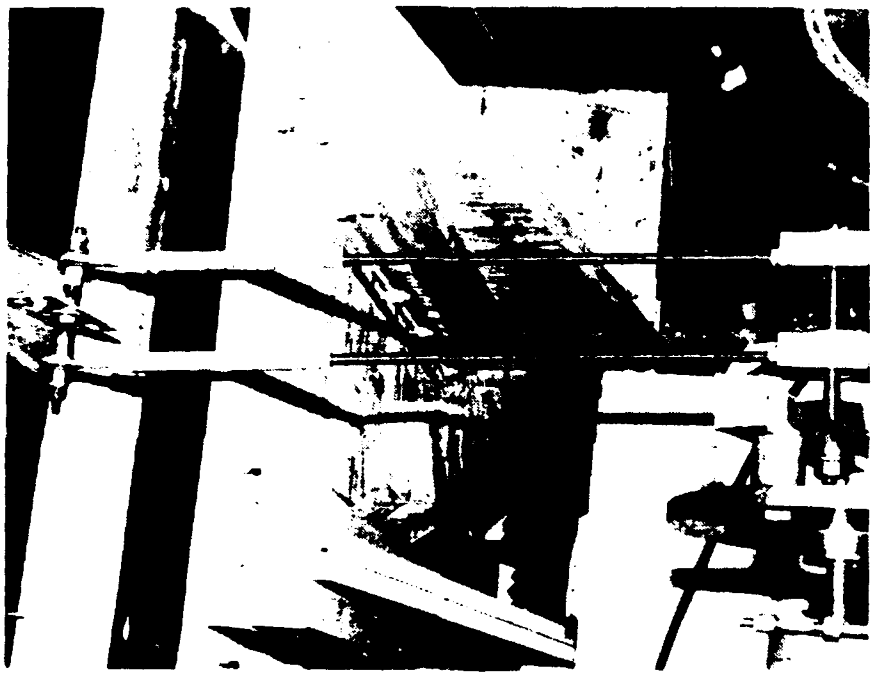

Figure 3.6. Yarber wave plunger.

The ten inch flywheel and plunger rod assembly were removed from Medwin's wave driver and connected to this system. The plunger rods are attached to the flywheel using a new (12 x 2 $\frac{3}{4}$ x 1 inch)(l x w x t) slotted aluminum adapter. The slotted adapter provides a continuously variable adjustment of the driving amplitude. The plunging system was mounted to a one cubic foot wooden

box, that was clamped to a cement laboratory table. The cement table was placed as close to the tank as possible.

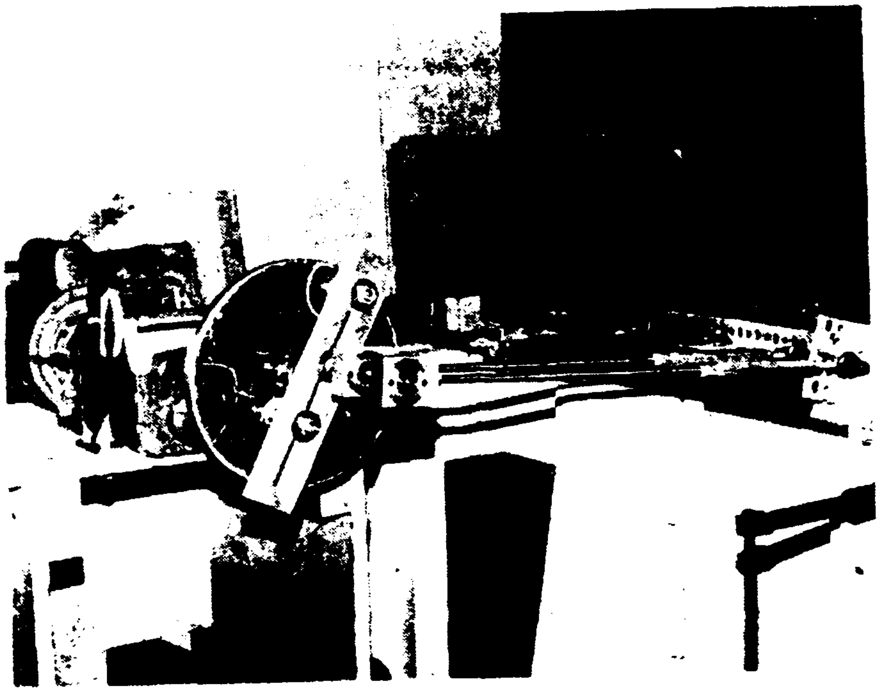

Figure 3.7. Yarber drive system.

The Yarber wave driver would change frequency at a rate of approximately 0.002 Hz per minute (B2P61) when the system ran continuously for over two minutes due to overheating in the mechanical speed adjuster. The amplitude and frequency were not adjustable during a measurement. This combination of things caused us to develop a third drive system.

c. Keolian Wave Driver

The Keolian wave driver is also continuously variable in both frequency and amplitude. It uses the same

forcing paddle assembly as the Yarber wave driver and an electric plunging system.

The plunging system consist of a function generator, power amplifier, electric shaker, and a single plunging rod assembly shown in Figure (3.8). A HP-3314A function generator is connected to an Acoustic Power Systems, Inc. APS-114, dual-mode power amplifier. The amplifier is operated in the current mode. The amplifier is connected to an APS-113 Electro-SELS® shaker. A Kikusui, COS-5060A, 100 MHz oscilloscope is used to monitor the amplifier input and output.

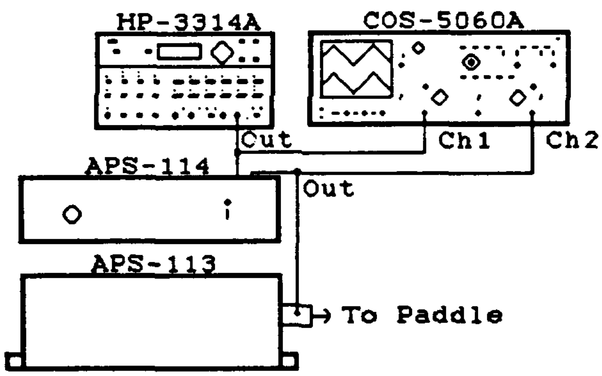

Figure 3.8. Keolian drive system.

The plunging rod assembly consist of a 14.5 inch, $\frac{3}{8}$-16 threaded rod with a one inch ball joint on each end. One ball joint was connected to a three inch aluminum L-bracket, which was bolted to the shaker using $\frac{1}{2}$ inch long, $\frac{1}{4}$-20 bolts. The other ball joint was connected to a L-bracket on the paddle.

The wave amplitude and frequency are easily adjusted at any time using the synthesizer/function generator. Complex wave forms and noise can also be applied to the paddle using the amplifier and shaker. This will be important in latter experiments.

5. Surface Drag Measurements

Surface drag measurements were made at various wind speeds, approximately four feet from the wind insertion point, at location two in Figure (3.2).

A special apparatus was constructed to hold the wires and associated electronics of the capacitive probe setup in the tank. We call this apparatus the Harp. The Harp is constructed of two 47.5 inch long aluminum U-channels, connected by two 30 inch long, 1/2 inch diameter aluminum rods. The upper U-channel is 2.25 inches wide by one inch high. The lower U-channel is 0.9 inches wide by 0.6 inches high. The wires were mounted using number one rubber bands attached to one end of the probe and the lower piece of the Harp. The upper ends were attached to a guitar adjuster, which was mounted to a 1/4 inch Plexiglas strip that was connected to the Harp. An electronics box was screwed onto the Harp.

The Harp was put into the water with a single capacitance probe and a clear plastic ruler attached to the Harp with a three inch C-clamp. The ruler and probe were separated by ten centimeters at the air-water interface and

the line formed was normal to the wind direction. Lint was placed on the water upwind of the ruler. The dust travel time between the two points was measured using a Casio Alarm Chrono G-Shock digital watch. The measured surface drag speeds are reported in Table (3.1).

C. CALIBRATION TECHNIQUES

1. Introduction

There are two types of calibration techniques which were performed in this thesis. The apparatus and procedures for two calibrations will be described in this section.

The first type of calibration was a static calibration which was used primarily during the probe selection. Static calibrations were also conducted to establish system baseline sensitivities.

The second type of calibration was a dynamic calibration. The dynamic calibrations were the most important for the thesis because they set the sensitivity limits for the sensor system for all further measurements.

2. Static Calibration

The static calibration technique had three component parts as shown in Figure (3.9). The specific parts used as the water or electronics components could be changed, depending on the specific test conducted. A Starrett Co., No. 254, 26 inch master vernier height gage was used in all static calibrations.

The static calibration technique is simple. The sensor or sensor system was somehow attached to the height gage. The necessary measurement electronics were connected to the sensor or sensor system. The sensors were immersed in water. The sensor parameters or sensor system electrical outputs were measured, verses the measured relative immersion determined using the height gage. A sensitivity was then computed, in the form

$$\frac{\Delta \text{ output}}{\Delta \text{ height}}. \qquad \text{Eqn 3.1}$$

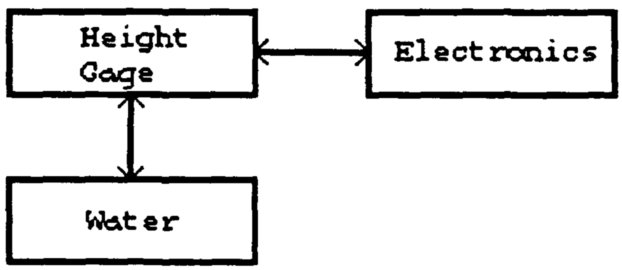

Figure 3.9. Static calibration components.

3. Dynamic Calibration

The dynamic calibration techniques also have three component parts as shown in Figure (3.10). All of these components could be changed depending on the specific test conducted, and components could be combined during certain tests. The dynamic calibrations were limited to sensor system tests.

There were two movement possibilities for the dynamic calibrations. The sensor system could be moved in

the water or the water could be moved past the sensor system. Dynamic calibrations for both movements were attempted.

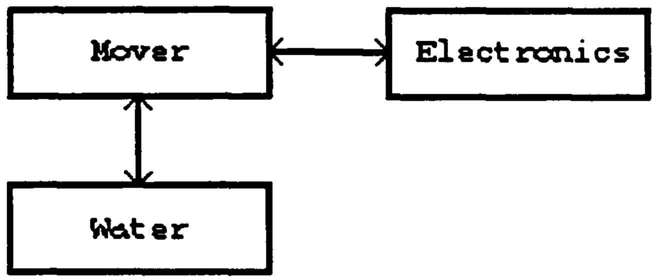

Figure 3.10. Dynamic calibration components.

A subjective decision was made that the best dynamic calibration was an dynamic calibration for a constant amplitude traveling water wave, moving past the sensor system. This decision was made because the traveling wave is a gravity wave. Gravity waves and wind-water waves were what the sensor system was designed to measure. The other dynamic calibration techniques attempted are described fully in Appendix B.

The sensor system was placed in the small wave guide describe in chapter III-B-2-b. A static calibration was conducted to establish the baseline sensitivity. A 12 inch long, 0.031 inch diameter brass rod was scotch taped to a Starrett Co., No. A LH, three axis micrometer. The micrometer was bolted to the main tank approximately three feet from the paddle and directly above the small wave guide.

The brass rod was raised 0.354 cm above the unperturbed water. This would provide a visual point with a 0.25 cm RMS maximum for the traveling waves.

The Keolian wave driver was attached to the paddle of the small wave guide. The drive amplitude was adjusted so that the traveling wave amplitude was constant, ± 0.1 cm, as determined by the peaks of the wave just touching the bottom of the brass rod for several frequencies below 4.0 Hz. The small wave guide cutoff for the paddle generated parametric waves was 3.95 Hz which limited the frequency of the calibration. The sensor system electrical output for a constant amplitude traveling wave was measured, verses applied drive frequency. A sensitivity was then computed, in the form

$$\frac{\Delta \text{ output}}{\Delta \text{ frequency}}. \qquad \text{Eqn 3.2}$$

D. WAVE HEIGHT PROBES

The second experimental component is the wave height sensor probe that we need to make the surface gravity wave measurements. The goal is to develop a height sensor that is linear, very sensitive, and noise immune. A variety of wave probes have been used by experimenters using changes in capacitance and resistance [Ref. 5, 7]. Two sensor probes were tested in this investigation. The constraints in the probe selection, test procedures, results, and final probe selection will be discussed in this section.

1. Capacitance Probe

The capacitance probe investigated in this thesis utilized the two-wire measurement technique described earlier. The variable capacitance measured is determined by the probe immersion into water. The capacitance probes were all labeled and marked T-(#) so that repeated measurements could be made for analysis for each probe. The probes were placed on the Harp for all capacitance test conducted in the wind-wave tank.

There were two major categories of constraints on the capacitance probe selection. Optimizing the various electrical and hydrodynamic constraints was an interesting challenge.

There are three electrical constraints on the probe when it is in the water. The first constraint is that the resistance between the probe and water should be nearly infinite.

The second constraint is that the capacitance per unit length should be as high as possible to maximize the sensor sensitivity. From equation (2.15), the capacitance increases as the radius of the outer charged surface approaches the radius of the inner charged surface. We wanted as thin a dielectric as possible. Meeting this constraint would establish an "ideal" electrical capacitive component.

The third constraint is that the capacitance sensitivity, should be constant over the length of the cylinder, to remove unwanted systematic errors. This required a uniform dielectric.

There were also two interrelated hydrodynamic constraints on the probe that also require optimization. The first constraint was that the probe drag needed to be minimized to reduce the induced turbulence in the flow field, caused by the probes. This also required a thin conductor and dielectric. Second, the effect of probe wetting needed to be minimized so that the change of capacitance closely followed the water height, reducing hysterisis.

The optimization of the hydrodynamic constraints had to be accomplished on two time scales. The period of a forced surface gravity wave is the first time frame. This time frame is important, as it sets the low frequency limit of the sensor. The period of an experimental data run is the second time frame. The capacitance sensitivity, must remain constant during this time frame to prevent systematic errors in the measurements.

Finding the right sensor seemed like it would be an easy job. First we needed to find an electrical conductor that had nearly infinite resistance, that could be used as a conductor/dielectric/water capacitor.

Determining what wire should be used was the first order of business. The first test was to find a linear and highly sensitive probe. The static calibration technique discussed in chapter III-C-2 was used to measure the probe sensitivity. The sensor probes were submerged in water taken from the tank and contained in a (2.25 x 17.5 inch)(diameter x h), 1000 ml, Pyrex™ graduated cylinder. The capacitance of a submerged probe was measured using a HP 4192A LF Impedance Analyzer.

Measurements were made with the HP-4192A using a 30.0 kHz, 1.0 volt drive signal. The 30.0 kHz signal is used because comparable frequencies will be used in latter experiments. A 5.0 ounce plum bob is used to straighten the probe and insure that it is perpendicular to the air-water interface. Figure (3.11) is a diagram of the experimental apparatus.

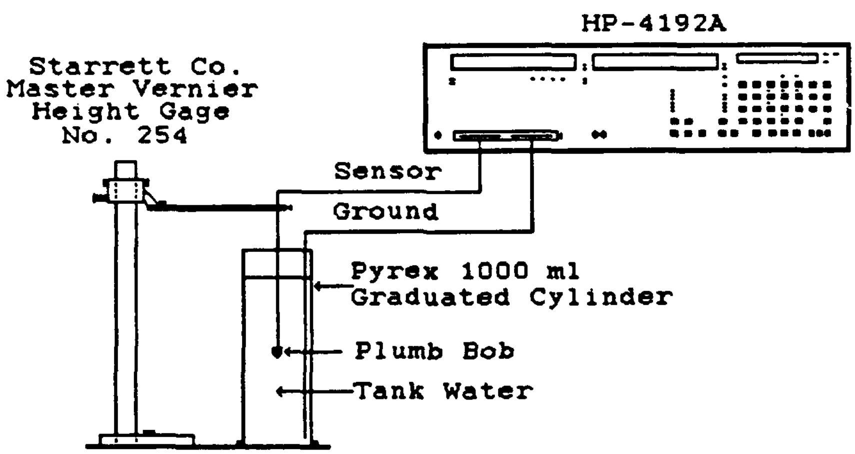

Figure 3.11. Static capacitance sensitivity experimental setup.

The first capacitance probes that were tested were all made from magnet wire. Several coatings were tested on the magnet wire. There were eight probes built, using 22 gauge magnet wire manufactured by Belden and Consolidated. The ends of half the probes were dipped in blue Testors model paint. The ends of the other half of the probes were coated in BIPAX, TRA-BOND, BA-2106, 5-minute epoxy. Half of the probes were coated in Bulls Eye Shellac, while the remaining probes only had their manufacturer's insulating coating. Neither the capacitance nor the dissipation were constant, at a constant immersion depth, for a length of time comparable to an expected gravity wave measurement.

A second capacitance probe was built, but not fully tested because the measurement technique was changed. A 33 inch long, 0.160 inch ID., and $\frac{1}{4}$ inch OD. glass capillary tube formed the dielectric for this probe. A Malco S-50 Micro dot connector, P.N. 031-0001-0001, was soldered to 22 gauge tin copper wire (Aztec Wire & Cable). One end of the glass was melted closed and the wire was place in the capillary tube. The connector end of the wire was attached to the glass with several layers of shrink tubing.

The final wire tested and selected for use was Omega Engineering, Inc., TF-010, 10 mil diameter, Teflon coated copper thermocouple wire. The Teflon has a dielectric constant $K = 2.0$ to 2.1 [Ref. 31]. It was selected for the sensor probe because its capacitance was constant over time.

Figure (3.12) shows measurement samples of capacitance verses time for shellacked magnet wire (T-2) and Omega thermocouple wire (T-15). The shellacked magnet wire capacitance changed at a rate of 4.5 $\frac{\text{pF}}{\text{min}}$. The Omega thermocouple wire capacitance changed at a rate of 0.013$\frac{\text{pF}}{\text{min}}$.

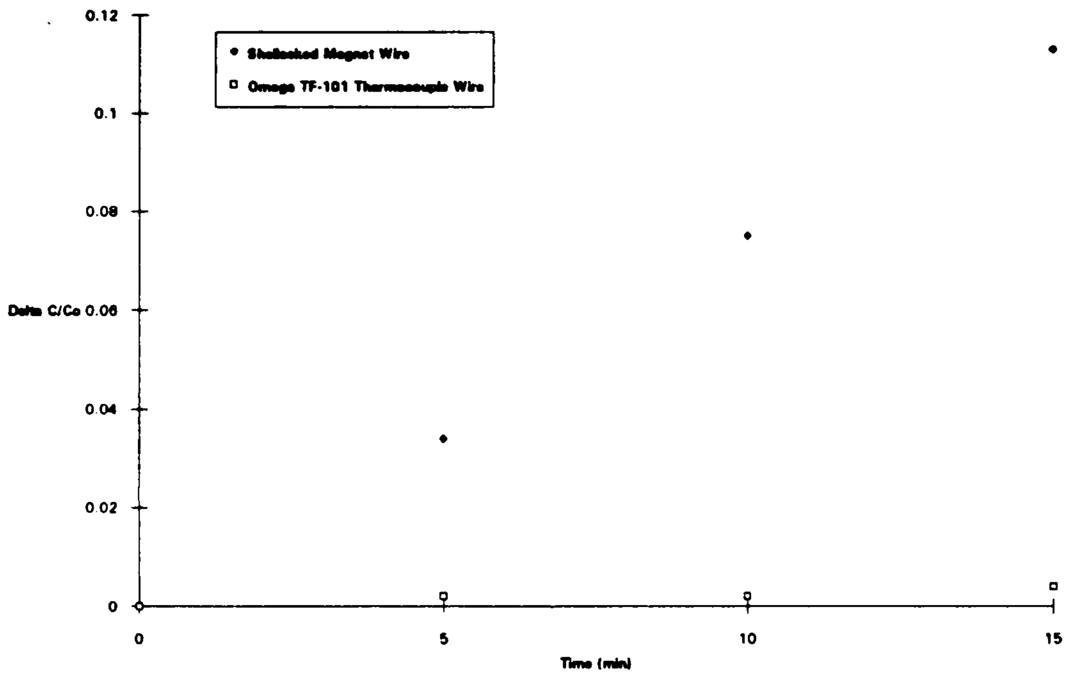

Figure 3.12. Capacitance of immersed probe wire vs. Time (B1P36).

The immersed end of the Teflon wire was looped and tied to the plum bob or other tensioning device. The knot was covered with Polymeric Systems, Inc., PSI 601 Clear, 100% Silicone, RTV Adhesive Sealant. Approximately $\frac{1}{2}$ inch of electrical heat shrink tubing was shrunk over the knot and RTV. The "dry" end of the probe was tinned and soldered into a male, 0.062 inch, terminal (Digi-Key part number WM1000).

Test were performed in tank water and in mercury using the static equipment setup shown in Figure (3.4). The mercury was held in a different container for safety reasons. The mercury test should give results as close to theory as experimentally possible.

The theoretical capacitance per unit length for this geometry using equation (2.15) is $C_{theory} = 2.40 \pm 0.01$ pF/cm (B2P73). The measured capacitance sensitivity was 2.2 ± 0.1 pF/cm in mercury and 2.4 ± 0.1 pF/cm in tank water, as shown in Figure (3.13), and was linear as a function of immersion in both cases.

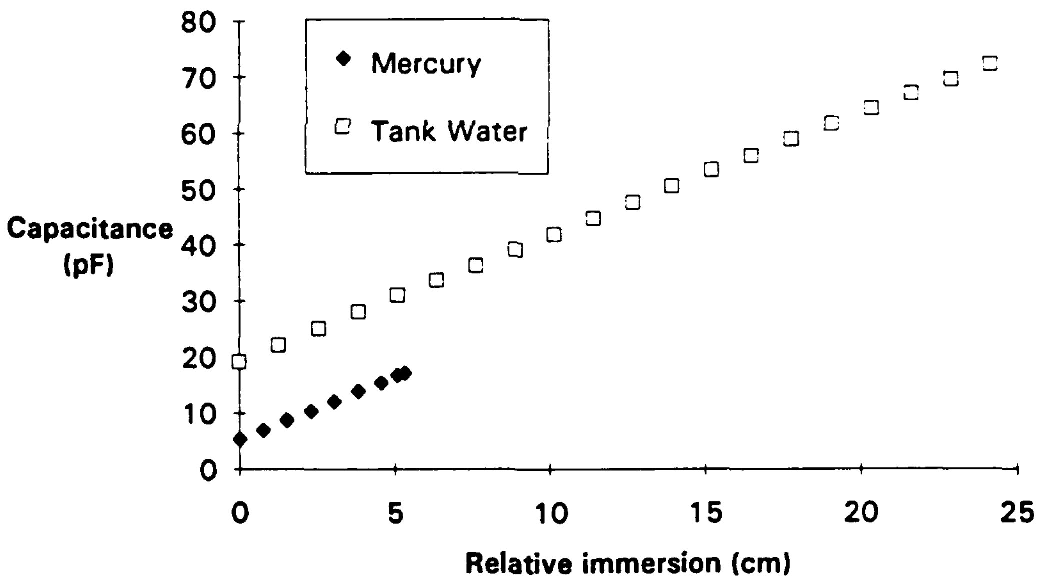

Figure 3.13 Capacitance of Teflon wire in different media vs. Relative immersion (B2P22/102).

A wire capacitance static calibration was performed in the wind-wave tanks using precision blocks for the height

gage. The blocks were 1.7 ± 0.1 cm high. The measured capacitance sensitivity for this test was 2.2 ± 0.1 pF/cm, as shown in Figure (3.14), and was linear as a function of immersion.

A final static capacitance sensitivity test was performed in the large wind-wave tank using a HP4194-A Impedance/Gain Phase Analyzer. The four wire measurement technique was used to measure resistance R and reactance X. The capacitance probe was on one side of the DUT, tank water, and the other side was the Harp or a paper clip.

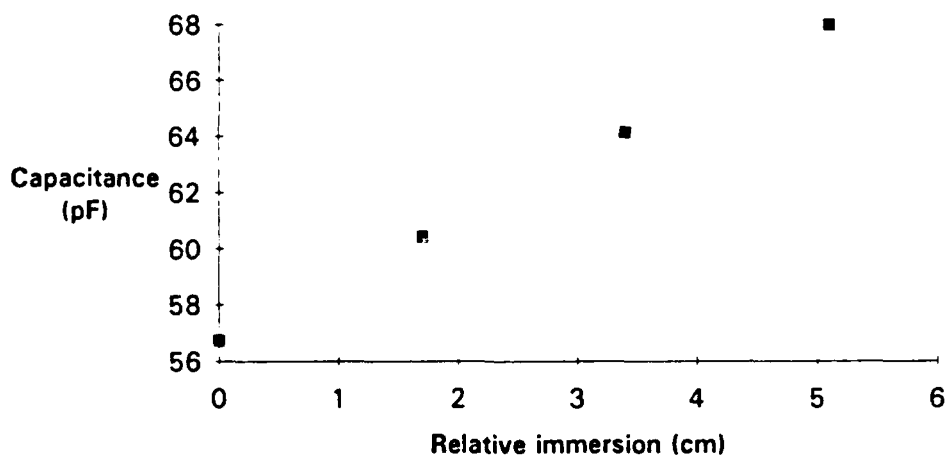

Figure 3.14. Capacitance vs. Relative immersion for T-15 using precision blocks (B2P108).

The capacitance can be determined for the measured reactance, as a function of frequency, [Ref. 31] by

$$C(f) = -\frac{1}{2\pi f X}. \quad \text{Eqn 3.3}$$

The probe wire was mounted on the Harp and immersed approximately 25.0 ± 0.5 cm. The theoretical capacitance for a cylinder of this length is 60.0 pF. The measured capacitance was 62.5 ± 0.1 pF at 30 kHz using the paper clip, and 66.5 ± 0.1 pF using the Harp, as shown in Figures (3.15 and 3.16).

The static capacitance sensitivities for the various measurement techniques are shown in Table (3.2). The measured sensitivities are in general good agreement with theory.

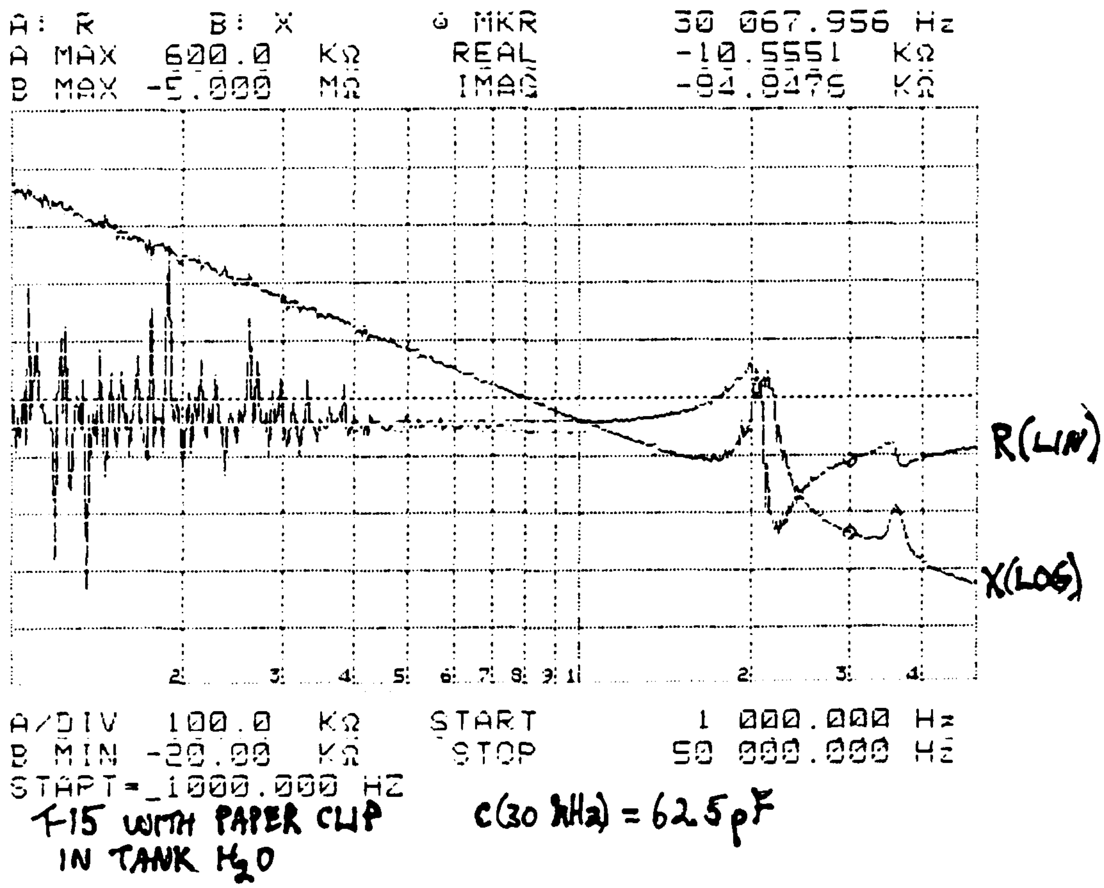

Figure 3.15. R & X vs. f for Teflon wire (T-15) in the wind-wave tank using a paper clip (B2P93).

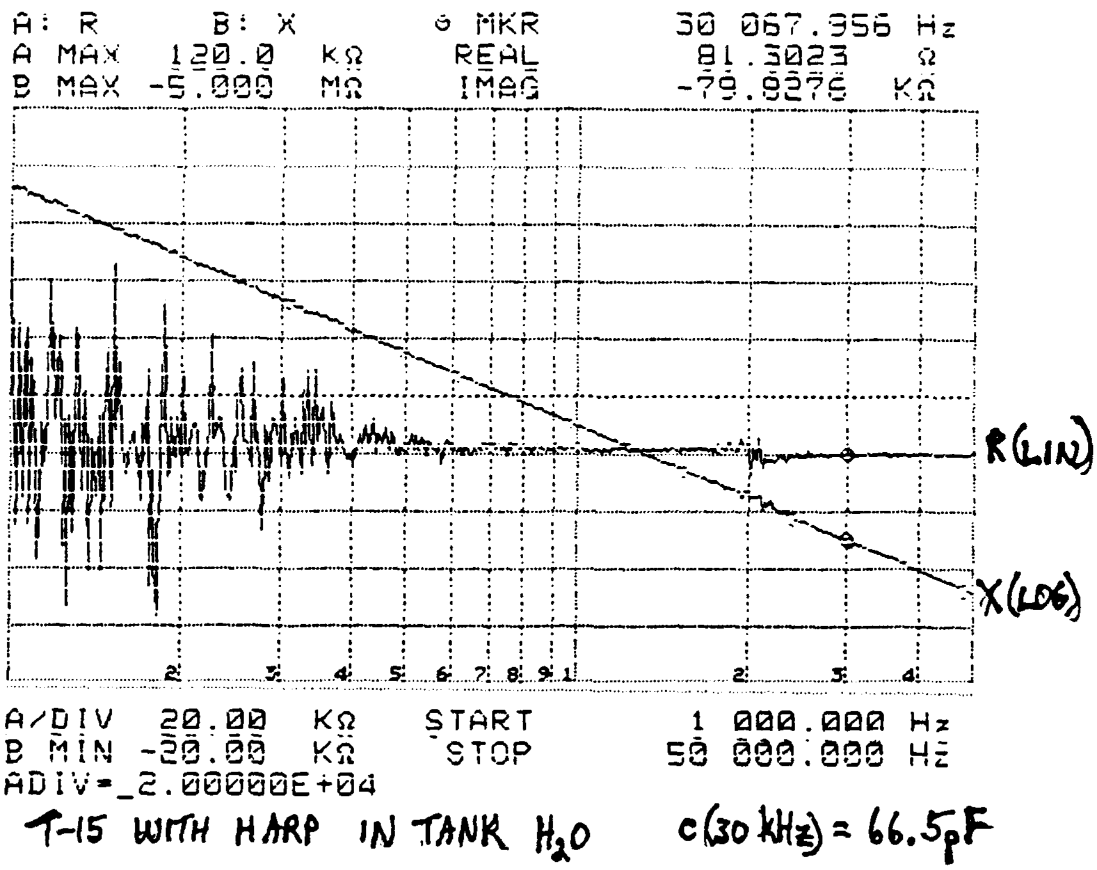

Figure 3.16. R & X vs. f for Teflon wire (T-15) in the wind-wave tank using the Harp (B2P93).

TABLE 3.2. STATIC CAPACITANCE SENSITIVITIES FOR ALL MEASUREMENT TECHNIQUES.

Method	Sensitivity (±0.1 pF/cm)
Cylindrical Theory for TF-101	2.4
T-13 immersed in graduated cylinder with tank water at 30 kHz (B2P23)	2.2
T-15 immersed in graduated cylinder with tank water at 30 kHz (B2P23)	2.3
Omega TF-101 in Mercury (B2P102)	2.2
T-15 immersed on Harp in wind-wave tank using precision blocks (B2P108)	2.2
T-15 immersed on Harp in wind-wave tank at 30 kHz, Harp ground (B2P93)	2.7
T-15 immersed on Harp in wind-wave tank at 30 kHz, paper clip ground (B2P93)	2.4

2. Conductance Probe

The idea of a four wire measurement was motivated by continued electrical grounding problems in the tank when using the capacitance probe and the inability to accurately measure the electrical properties of water. The four wire technique was described in chapter II-D. It was not obvious however, what quantity should be measured. This section will describe how we decided to measured conductance and the selection process for the best conductance probe.

The type of measurement was the first item to be determined. The static calibration technique discussed in chapter III-C-2 was used for these test. Tank water was placed in either a 1000 ml Pyrex™ graduated cylinder or a four liter desiccator. The BNC cables were connected to a HP-4194A Impedance/Gain-Phase Analyzer in the four wire measurement mode. A Think Jet printer was connected to the analyzer by HBIB bus for data recording.

A (11.5 x 43.0 cm)(l x w) Vector perforated printed circuit board had 20, number 43 holes, drilled 0.125 inches from one end. The holes were 0.0125 inches apart so that $\frac{1}{4}$ inch, 2-56 stainless steel machine screws could be placed in the board. These machine screws became the restraining mechanism and electrical connectors for the various samples. Two BNC cables were tied to the Vector board. Two Kings, KC-79-35, E-Z mini hooks were then attached to the machine screws and BNC cables. The Vector board was clamped to a

Starret Co., No. 254, master vernier height gage with a one inch C-clamp. The experimental setup is shown is Figure (3.17).

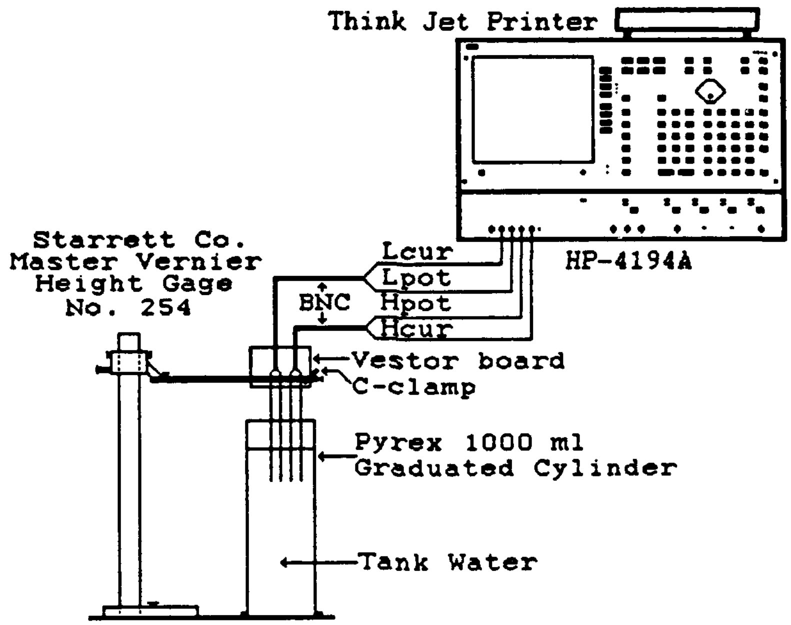

Figure 3.17. Conductance experimental test setup.

Resistance R, reactance X, conductance G, and susceptance B, were all measured as a function of wire immersion. A 30 kHz, one volt signal was used to drive the four 0.0195 inch diameter brass wires that were 0.125 inches apart. Brass was used only because it was most accessible at the time. Conductance proved to be linear as shown in Figure (3.18), which is the type of measurement we want.

The next test, using the same equipment setup, was conducted to determine what kind of metal and sensor geometry was best, if there was a frequency dependence, and if there was any dependence on drive signal or time.

Using a swept frequency in two ranges, 100 Hz to 50 kHz and 100 Hz to 2 MHz, R, X, G, and B were measured as a function of depth for each probe. This provided a check for any frequency dependence in the measurement. Typical test measurement data is shown in Figures (3.19 & 3.20). The x and y axis are both linear in all cases. There is no frequency dependence evident.

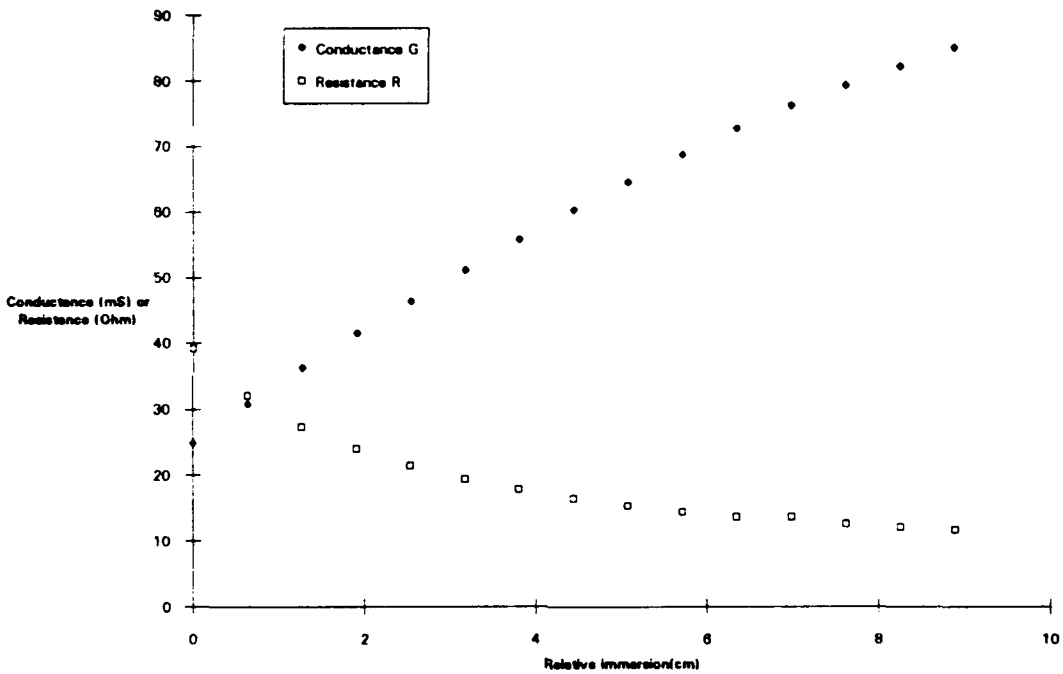

Figure 3.18. Brass wire G & R vs. Relative immersion (B2P118).

Brass, gold, platinum, and stainless steel were tested in a V shaped or cylindrical geometry. The brass were (10.4 cm x 0.288" x 0.005")(l x w x t) V shaped strips and 0.195 inch diameter, 10.4 cm long wires. The gold was 0.20 inch diameter, 8.9 cm long wires. The platinum was (16.5 x

0.68 x 0.032 cm)(l x w x t) V shaped strips. The stainless steel was 0.20 inch diameter, 10.2 cm long wires.

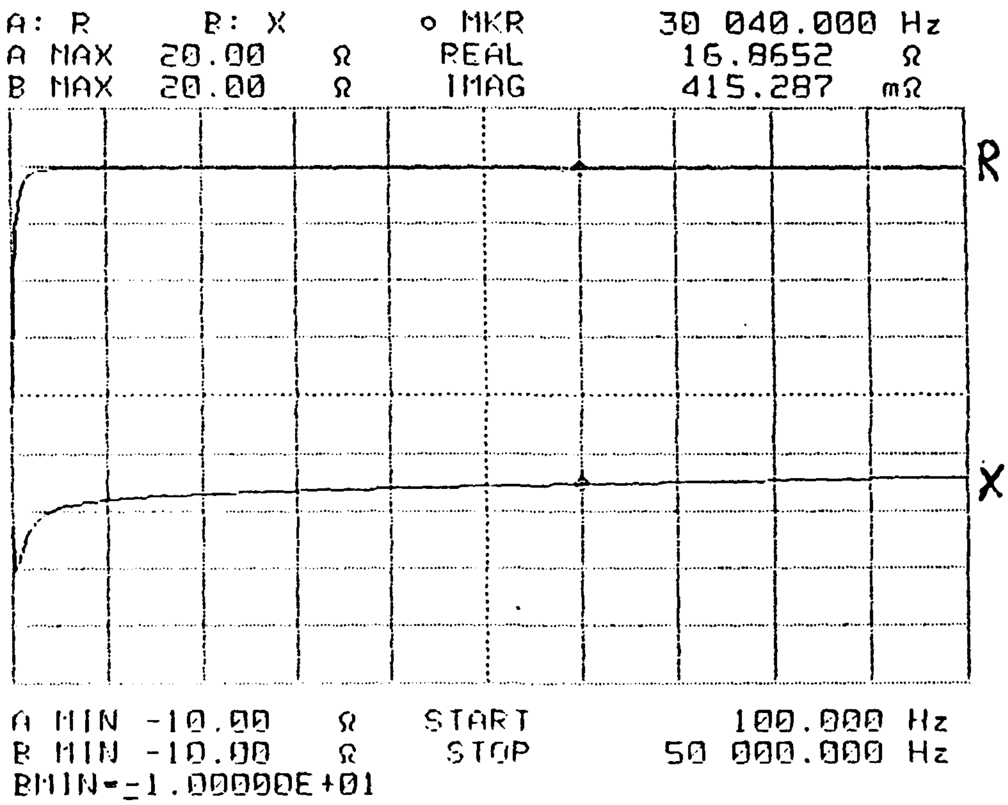

Figure 3.19. R & X for a stainless steel wire at a 6.0 cm relative immersion vs. Frequency (100-50,000 Hz).

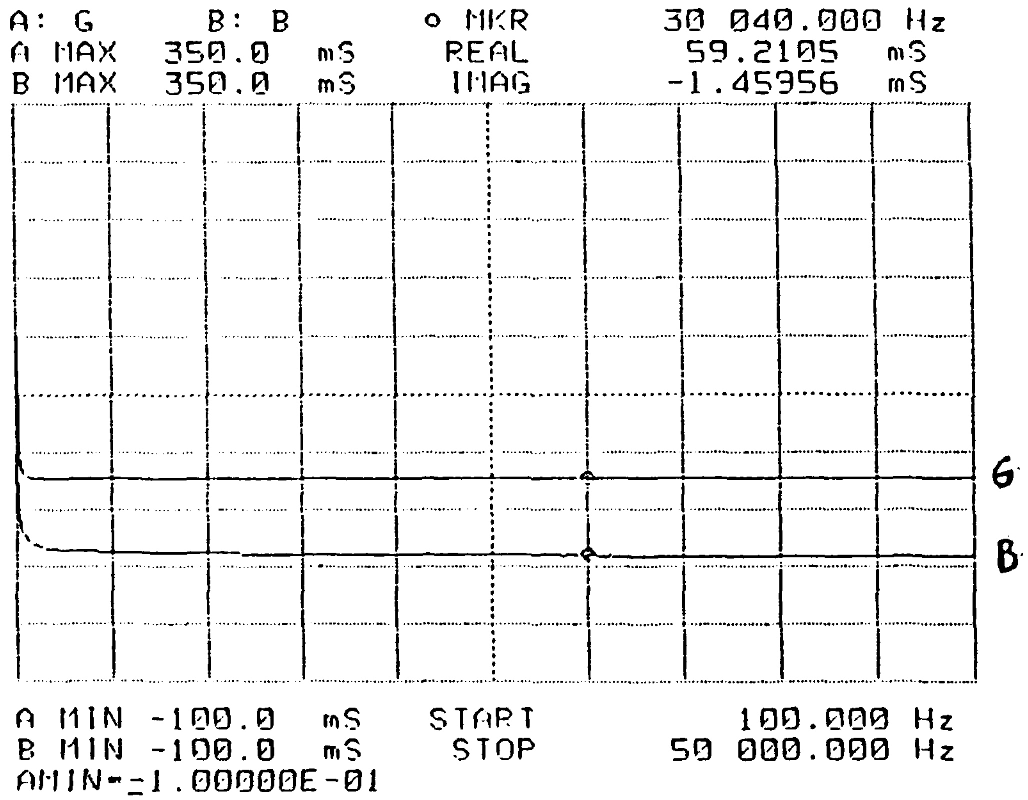

Figure 3.20. G & B for a stainless steel wire at a 6.0 cm relative immersion vs. Frequency (100-50,000 Hz).

The stainless steel wire had the highest sensitivity of the metals tested, at 8.4 $\frac{mS}{cm}$. The brass wire had a higher sensitivity than the brass strip. We decided to use stainless steel wire because of its high sensitivity. A plot of the measurement data is shown in Figure (3.21).

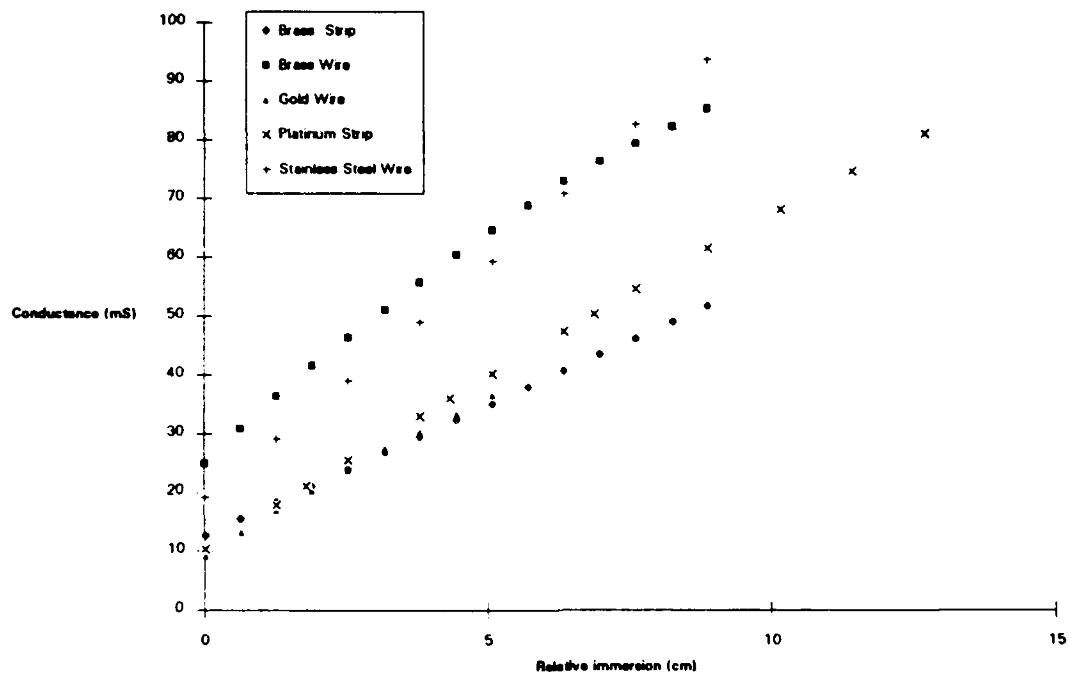

Figure 3.21. Conductance of four metals and two geometry's vs. Relative immersion (B2P114-119).

Figure (3.22) shows that there is no dependence on oscillator drive for brass or stainless steel wires, at a constant immersion depth of approximately seven centimeters.

The final test for the conductance probe wire selection was to determine if there was a time dependence for the stainless steel wire. There is a very small dependence of $0.01\frac{mS}{min}$, shown in Figure (3.23).

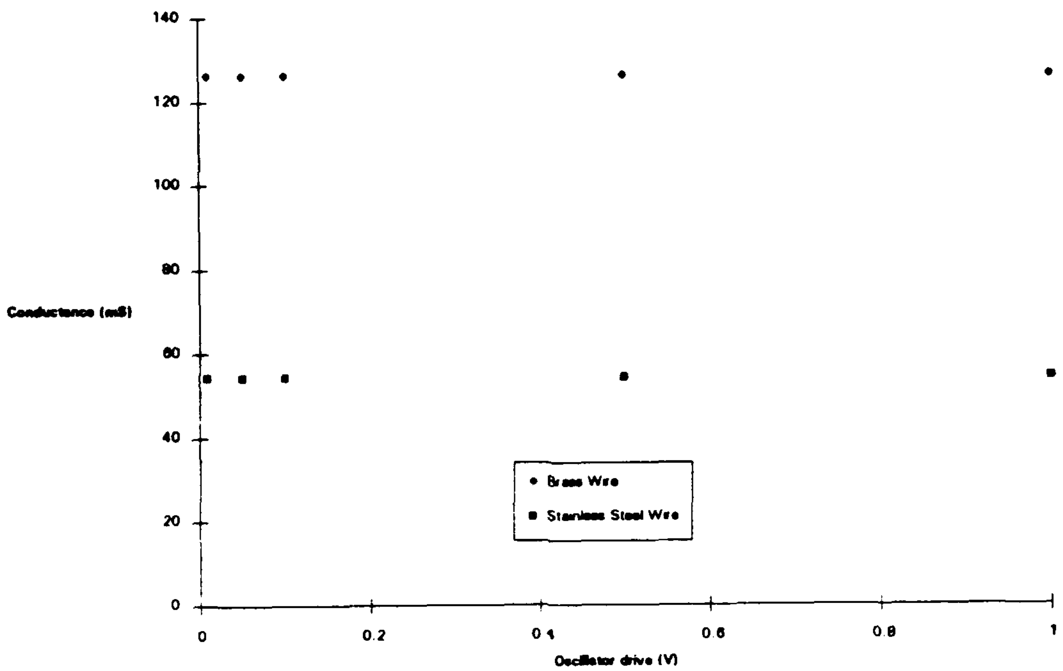

Figure 3.22. Conductance of two metals vs. Oscillator drive (B2P148).

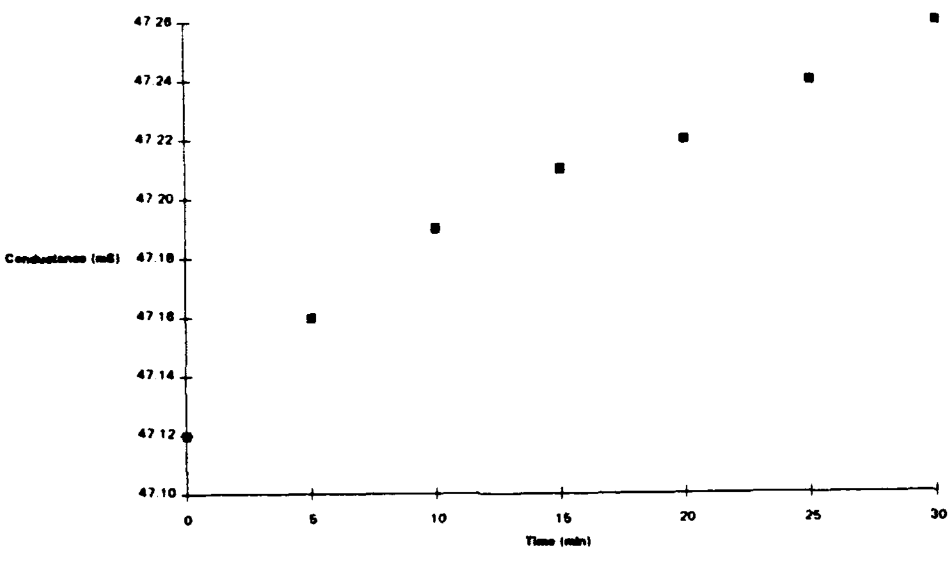

Figure 3.23. Conductance of stainless steel wire vs. Time (B2P149).

A five wire configuration of stainless steel wire was tested and selected for use in the conductance method. This configuration was selected for the probe because two separate two wire measurements could be made simultaneously at approximately the same location. It was anticipated that the two outputs might be used in a gradient measurement.

The probe has five, 0.020 inch diameter, five inch long stainless steel wires that are held at the top by a (1.5 x 1 inch) Vector board, and held at the bottom by a (1.5 x 3/8 inch) double sided copper printed circuit board (PCB). Five 0.020 inch diameter holes were drilled 1/4 inch apart, in a line, on both the PCB and the Vector board.

A Dremel® Moto-tool®, model 395, was used to cut electrical pads for each hole on both sides of the PCB. The stainless steel wires were inserted in the holes of each board. The wires were then soldered on each side of the PCB. A 1/4 inch diameter semi-circular loop was formed at the top end of the wire, and one end was soldered into a Vector board hole along with a 20 inch long, 22 gage, wire used to make electrical connection to the associated electronics. The loop was used to adjust the tension of each individual stainless steel wire.

A 2.5 inch diameter "J" was formed on one end of a 20 inch long, 1/8 inch diameter, brass rod. The short side of the J was inserted into a 1/16 inch hole in an

electrically isolated pad on the PCB and soldered on both sides.

A two inch right sided triangular sheet of brass was soldered to the other end of the brass rod. A two inch long, 8-32, brass bolt was soldered to the opposite side of the triangular sheet. The screw was inserted into a 1/4 thick piece of Plexiglas which supported the Vector board. The Plexiglas gave the top of the probe some rigidity. A 8-32 brass nut was used on the bolt to adjust the tension on all five wires.

The brass rod was bolted to a 3/4 inch diameter PVC pipe. The 20 inch wires were fed through the PVC. The PVC could then be clamped and the conductance electronics could be mounted to the other end of the PVC. The five wire probe is shown in Figure (3.24).

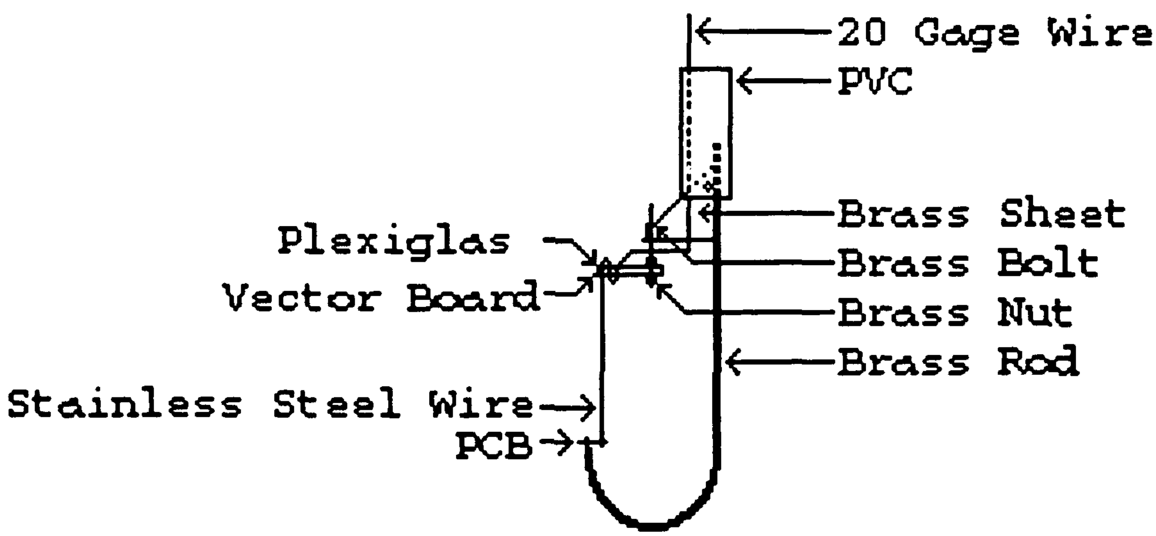

Figure 3.24. Five wire probe construction.

E. MEASUREMENT SYSTEM ELECTRONICS

The third experimental component is the associated electronics, which will convert whatever the sensor is measuring into a usable electric signal. This component must also be linear, sensitive, and immune to noise. The constraints and design for the electronics, test procedures, results, and final electronics selection will be discussed in this section.

1. Capacitance System Electronics

The capacitance system electronics is a two channel, capacitance bridge, op-amp circuit. The purpose of this circuit is to provide an electrical output for the sensor probe by converting the capacitance changes of the probe wire into voltage changes which could be input to conventional electronic signal processing instrumentation. The two sections of the circuit must combine to give a very sensitive and linear output which represents the height of the wave on the sensor probe.

The first section of the circuits are the transformer fed capacitance bridge, as shown in Figure (3.25), which provides a means to detect small signals. A lock-in amplifier oscillator output is fed into the bridge via transformer T1. The transformers are manufactured by ADC, model number TF4RX17YY. They have a frequency range from 40 Hz to 100 kHz.

The sensor probe and water ground form one leg of the bridge, variable capacitor C_{probe}. The other leg has three capacitors in parallel, one fixed value C1, and two variable value. There is a rough adjust C5 and a fine adjust C4. The variable capacitors are used to electrically null the bridge when the sensor is in the tank water and the water is in an equilibrium state. The bridge can also be nulled when a dummy load capacitor is inserted into the circuit instead of the tank water.

The typical equilibrium capacitance of the sensor probe is approximately 60 pF. The other leg of the capacitance bridge is the sum of the fixed, rough adjust, and fine adjust capacitors. The rough adjust capacitor has a value of 27 ± 13 pF. The fine adjust capacitor has a value of 10 ± 5 pF. The fixed capacitor in the adjustment leg is then

$$C_{fixed} = C_{sensor} - C_{rough} - C_{fine}. \qquad \text{Eqn. 3.4}$$

The approximate value for C_{fixed} is 23 pF.

The second section of the circuit provides output impedance matching and signal gain using an op-amp. The OPA-111 op-amp is used with a gain adjust capacitor C6. The OPA-111 provides a typical open-loop gain of 120 dB and typical common-mode rejection of 100 dB. Complete characteristics are found in the manufacture's specification sheet. [Ref. 32]

The two channels are identical except for the ground used after the transformer. The different grounds are used for circuit isolation and to minimize the channel cross-talk. The two channel outputs are matched and maximized using the gain adjust capacitor C6, in the op-amp feedback circuit.

The electronics had one linearity test. Linearity is the most important feature required for the dynamic wave height measurement system. The principle of superposition can be used if the sensor probe and electronic system components each have linear responses. The electronic system is measured using "dry" techniques.

The "dry" calibration of the electronic system is a lab bench experiment using mylar capacitors as a substitute for probe wire water capacitance. The values of these capacitors were all measured at room temperature using a HP-4192A Impedance Analyzer. The nine capacitors used for the dummy load test were measured and the results of this test are shown in Table (3.3).

A EG&G Princeton Applied Research, model 5210, Lock-In Amplifier was used as a signal source and detector. A 31.3 kHz, 1.999 volt signal was applied to the input of the electronic system. When both channels are being used, two lock-in amplifiers were used.

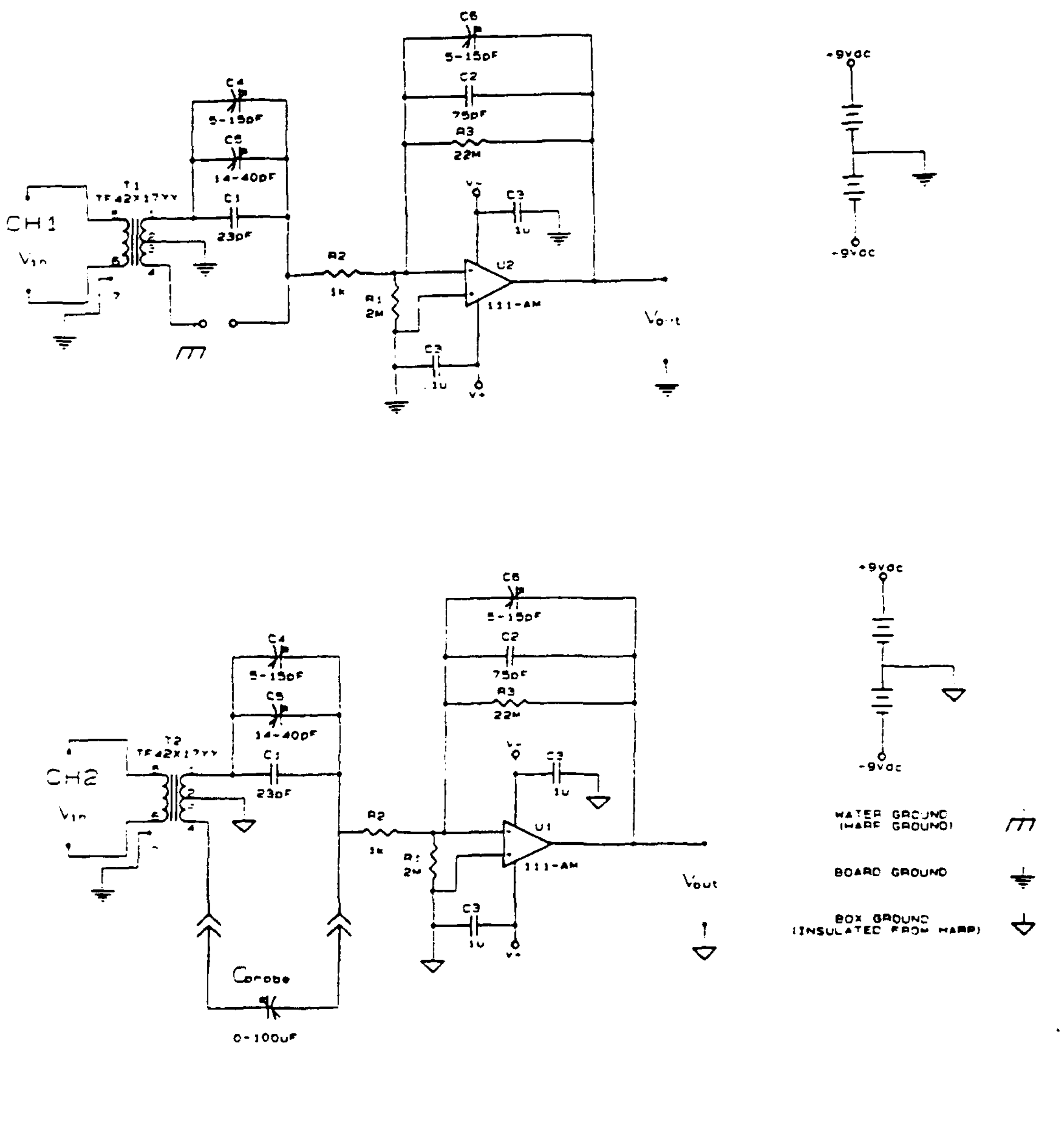

Figure 3.25. Capacitance system electronics circuit.

TABLE 3.3. DUMMY LOAD CAPACITANCE VALUES (B2P16).

Measured Capacitance (± 0.1 pF)
10.6
46.8
54.0
64.9
82.3
98.7
144.9
227.8
330.2
474.9

Different prime numbers are used for the frequencies of both lock-in amplifiers. We used 28.3 and 31.3 kHz throughout this experiment [Ref. 33].

The output of the electronic system was applied to the input of the lock-in amplifier. The typical lock-in amplifier setup configuration is shown in Table (3.4). A Kikisui, COS 5060, dual channel oscilloscope was used to monitor the electronics system input and output signals. Figure (3.26) shows a block diagram of the experimental setup.

TABLE 3.4. LOCK-IN AMPLIFIER SETUP CONFIGURATION.

Control Button	Setting
Sensitivity	300 mV
Filters	Flat & Tracking
τ	30 msec
Slope	12 dB
Dynamic Resolution	Normal
Display	XYV
Reference	Internal

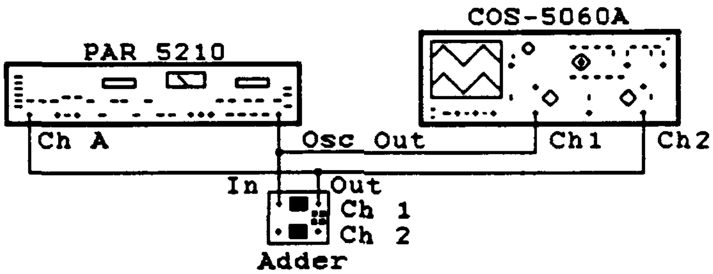

Figure 3.26. Dry electronic system experimental setup.

The first step of the dry calibration is to zero the bridge. The variable capacitor C4 and C5 are adjusted to zero the output voltage when a 54.0 pF dummy load capacitor is placed in each circuit.

The second step in the dry calibration is to match and maximize both channel outputs. Variable capacitor C6 is adjusted on both channels when a 10 pF dummy load capacitor is moved back and forth between the two channels. The output from a 450 pF range of capacitors is then measured to test the linearity of the electronic system.

Channel one sensitivity was measured at 3.21 ± 0.02 $\frac{mV}{pF}$. Channel two sensitivity was measured at 3.41 ± 0.03 $\frac{mV}{pF}$. The linearity for each channel is illustrated in Figure (3.27).

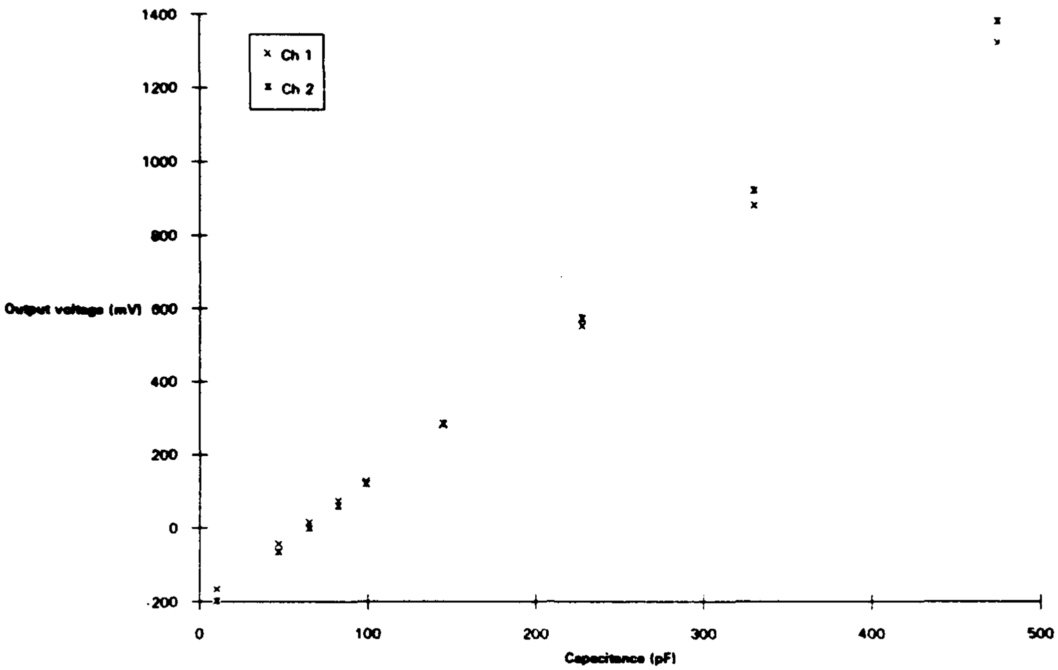

Figure 3.27. Capacitance system electronics output voltage vs. Dummy load capacitance (B2P17).

2. Conductance System Electronics

The five wire probe illustrated in Figure (3.24) is connected to two lock-in amplifiers to make a four wire water surface height resistance measurement, as shown in Figure (3.28).

Conductance is inversely proportional to the magnitude of the complex impedance, or ΔV, but is proportional to the water height on the probe as described earlier in Chapter II (C) (3). The conductance system electronics is a two channel division circuit. The purpose of this circuit is to invert and balance the two lock-in amplifier output signals. The two channels are identical

because we thought we might perform a gradient measurement using the difference outputs. Gradient measurements were not completed.

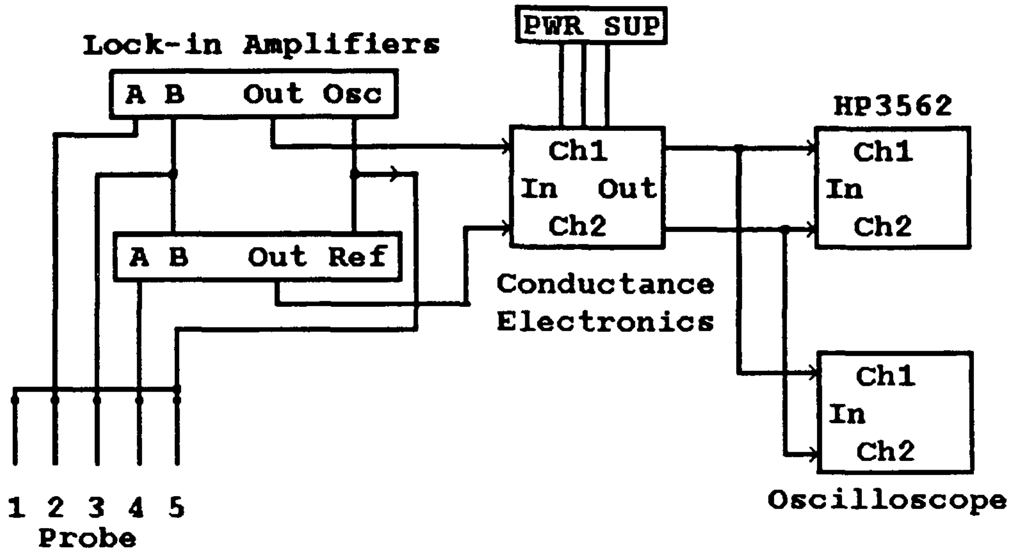

Figure 3.28. Five wire probe electronics setup.

The output voltage of a lock-in amplifier used in the differential mode, provides the input to an Analog Devices AD 534 Internally Trimmed Precision IC Multiplier, as shown in Figure (3.29). The output of the divider is determined by [Ref. 34]:

$$v_{out} = \frac{10\ z_2}{x_1} + y_1,$$

Eqn 3.5

where x_1 is the signal input, y_1 is the summing input, and z_2 is the numerator input.

Resistors R_1 through R_5 form a voltage divider network which determines the overall gain of both channels. Resistor R_3 is adjusted to equalize the two channel outputs for the same input signal. The circuit is powered by a KEPCO Multiple Output Power Supply, MPS 620M.

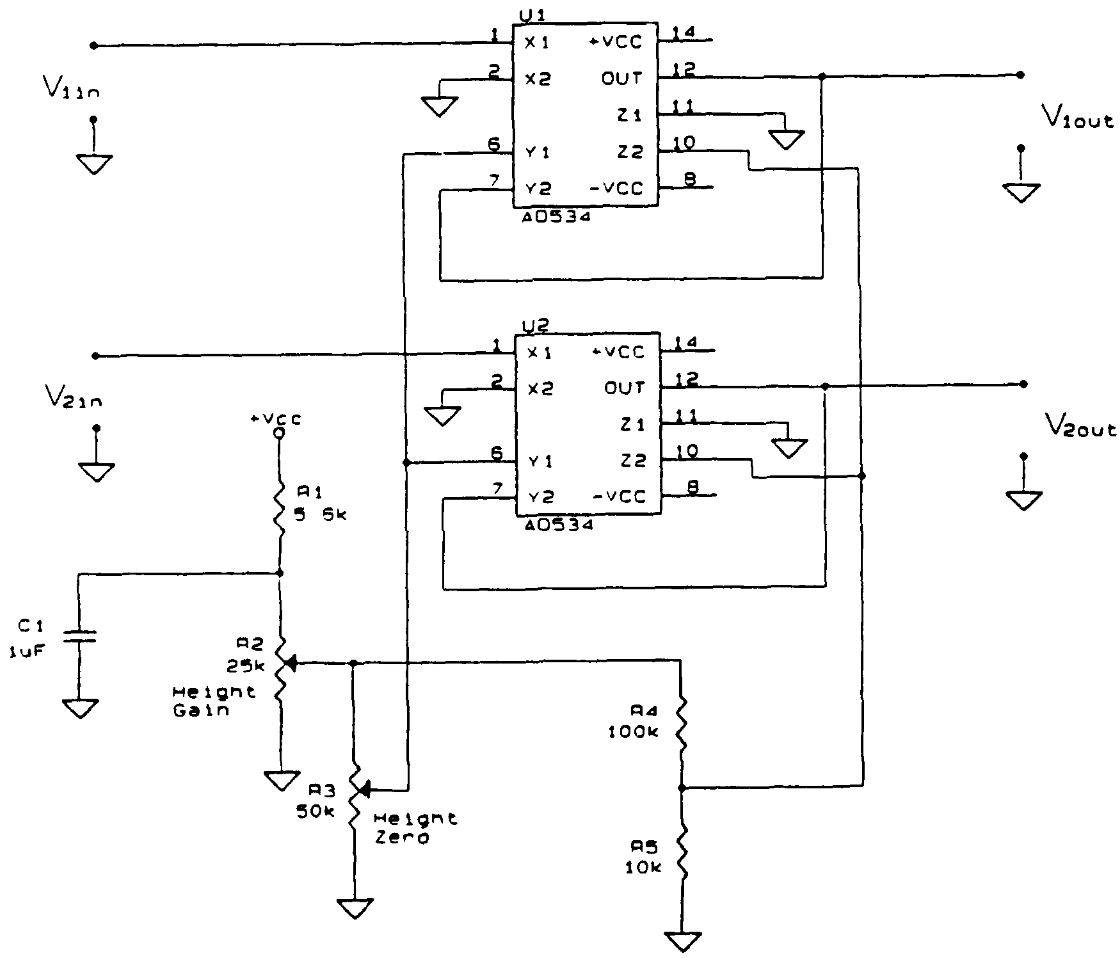

Figure 3.29. Conductance system electronics circuit.

F. WIND-WAVE TANK EXPERIMENTS

1. Introduction

There were five measurements made in the wave-wind tank. They were the wave power spectrum, surface gravity wave phase speed, surface gravity wave wavelength, and wave-wind tank system free decay Q and impedance measurements. This section will detail the apparatus and techniques used for each measurement.

2. Power Spectrum Measurement

All the wave-wind tank measurements except the tank impedance were based on the output of the power spectrum measurements as described in earlier sections. A signal was detected using either the capacitance or conductive measuring technique and then power spectrum measurements were made using a HP-3562A Dynamic Signal Analyzer. Measurements were made at various positions in the tank, and various wave-wind states. The basic states are:

a) baseline noise,

b) various wind speeds,

c) various driven surface gravity wave speeds, and

d) combinations of wind speeds and driven surface gravity wave speeds.

Data was recorded using a HP-7470A plotter or stored on disk using a HP-9133 hard disk. To store data on disk, the HP-3562A front panel control sequence in Appendix C was used. A HP-54501A, 100 MHz digitizing oscilloscope was used

to monitor the different electrical output signals. The experimental electronics setup is shown in Figure (3.30).

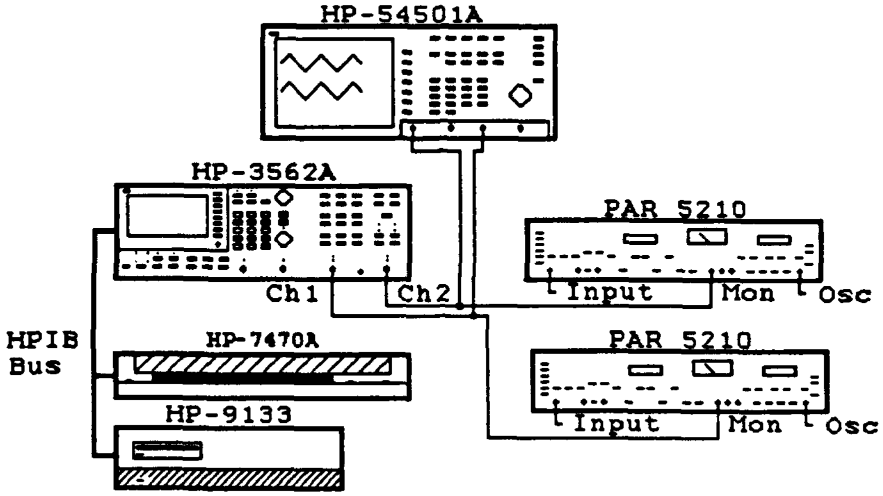

Figure 3.30. Measurement electronics setup.

Power spectrum measurements were taken with the HP-3562A using power spectrum measurement and display modes. Typical HP-3562A setup configurations are shown in Figure (3.31).

Log Resolution

MEASURE:	CHAN 1 Power Spec		CHAN 2 Power Spec	
AVERAGE:	TYPE Stable	# AVGS 5	OVERLAP 0%	OVFL REJ Off
FREQ:	START 1.0 Hz	STOP 100 Hz	SPAN 2 Dec	RESOLUTION 160 Pts
	REC LGTH 1.33 Min			
INPUT:	RANGE	ENG UNITS	COUPLING	
CH 1	AutoRng↑	7.65mV/EU	AC (Flt)	
CH 2	AutoRng↑	7.65mV/EU	AC (Flt)	
SOURCE:	TYPE Off		LEVEL 0.0 Vpk	OFFSET 0.0 Vpk

Figure 3.31. Typical HP-3562A power spectrum setup configuration.

3. Phase Speed and Wavelength Measurements

The phase speed and wavelength were measured using the cross-correlation output of the HP-3562A Dynamic Analyzer. Two signals had to be detected to make the phase speed measurement as described in chapter II-F using the experimental setup shown in Figure (3.30).

The HP-3562A computed and displayed the cross-correlation of the two signals. Typical HP-3562A setup configurations are shown in Figure (3.32). The Phase speed was then computed using the method of least squares fit on

the data output of the cross-correlation measurement. The distance between the two probes had to be measured, then the wavelength could be computed as described in chapter II-B.

Linear Resolution

MEASURE:	CHAN 1 Cross Corr		CHAN 2 Cross Corr	
WINDOW:	CHAN 1 Hanning		CHAN 2 Hanning	
AVERAGE:	TYPE Stable	# AVGS 10	OVERLAP 0%	TIME AVG Off
FREQ:	CENTER 10 Hz		SPAN 20.0 Hz	BW 37.5mHz
	REC LGTH 40.0 S	Δt 19.5mS		
TRIGGER:	TYPE Freerun	LEVEL 0.0 Vpk	SLOPE Pos	PREVIEW Off
INPUT:	RANGE	ENG UNITS	COUPLING	DELAY
CH 1	AutoRng↑	1.0 V/EU	DC (Flt)	0.0 S
CH 2	AutoRng↑	1.0 V/EU	DC (Flt)	0.0 S
SOURCE:	TYPE Rndm Noise		LEVEL 0.0 Vpk	OFFSET 0.0 Vpk

Figure 3.32. Typical HP-3562A cross correlation setup configuration.

4. Free Decay Q Measurement

The free decay Q was calculated using the power spectrum measurement output of the HP-3562A over a period of ten minutes. The ten spectra were measured one minute apart and stored on disk for each data set using the experimental setup shown in Figure (3.30), as described in chapter II-H.

The entire data set was latter plotted on the same paper. The data required for any measured frequency could be extracted from the data on the disk files, and the Q could be calculated.

5. Tank Electrical Impedance Measurement

A self contained mini experiment was performed to answer the question of why the lock-in amplifier oscillator was being loaded down by 5-50% during various capacitance measurements. The tank impedance, via the water and plumbing, returning to the rack ground was tested.

The lock-in amplifier output voltage was measured on an oscilloscope with and without the tank impedance in the circuit using the equipment setup shown in Figure (3.33). The tank impedance is then calculated using the measured voltage at any given frequency, by

$$Z_{tank} = \frac{V_{closed}}{V_{open}} Z_{LI}, \qquad \text{Eqn. 3.6}$$

where Z_{LI} is the lock-in amplifier output impedance. The lock-in amplifier has a 600 ohm output impedance which was verified with a 100 ohm resistor.

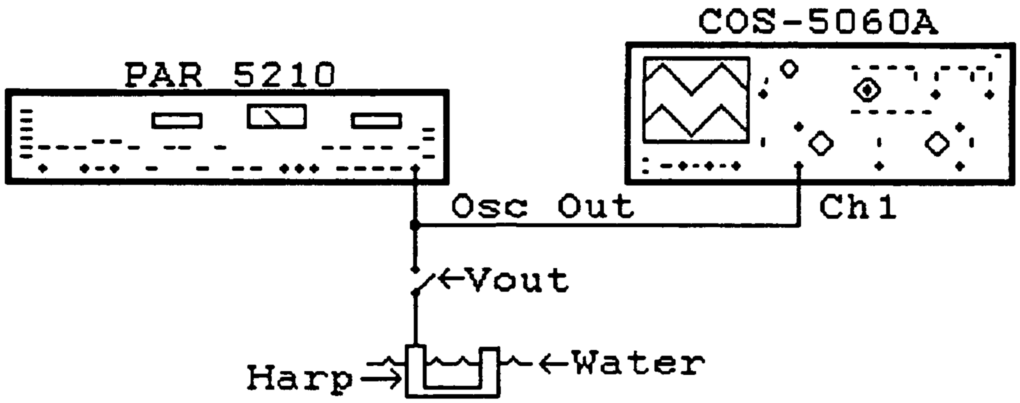

Figure 3.33. Tank electrical impedance experimental setup.

Voltage output for the closed circuit as a function of frequency is plotted and shown in Figure (3.34). The open circuit voltage was constant at 5.7 V_{pp}. The measured tank impedance at 20 kHz is Z(20 kHz) = 21.5 ohms.

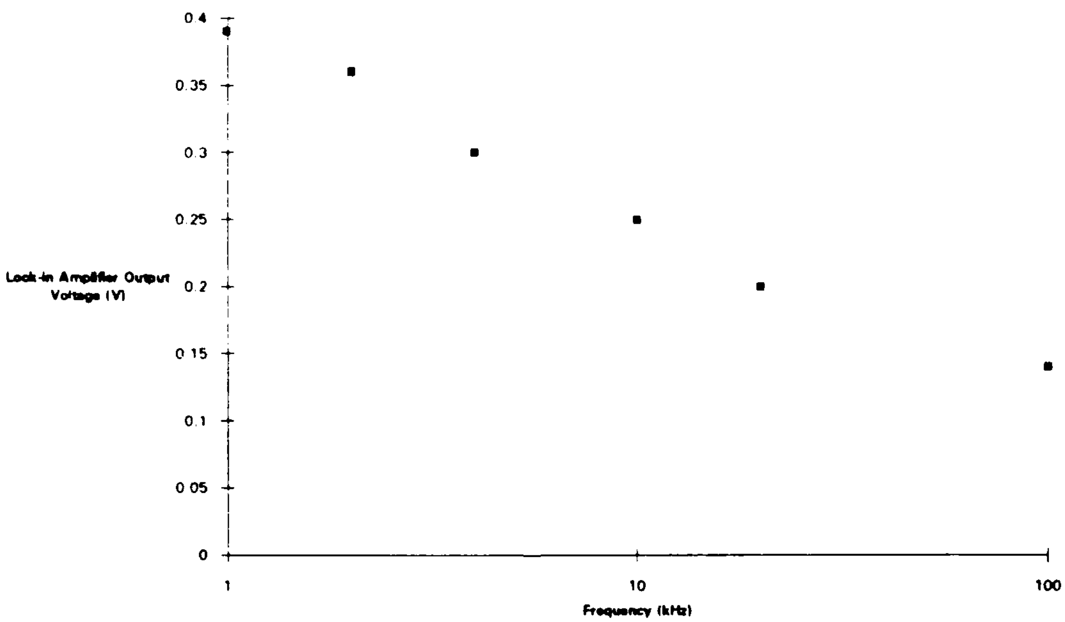

Figure 3.34. Lock-in amplifier output voltage vs. Frequency for tank (B2P107).

IV. RESULTS

A. STATIC CALIBRATIONS

The static calibrations were certainly the easiest measurement of the experiment. They were easy because there was no complicated equipment, the technique described in chapter III-C-2 is very easy to follow, and we used the static calibration technique so many times.

1. Capacitance Static Calibrations

All of the capacitance probe static calibrations were in good agreement with the theoretical capacitance sensitivity of 2.4 ± 0.1 pF/cm as shown in Table (3.2).

A theoretical capacitance system static voltage sensitivity could be determined by combining either the theoretical capacitance sensitivity or the measured Teflon wire capacitance sensitivity with the measured electrical sensitivities of each channel of the system electronics. The theoretical voltage sensitivities for each channel are shown in Table (4.1) using the results from the previous chapter.

Capacitance system static voltage sensitivities were measured using the static calibration technique with water contained in the Pyrex graduated cylinder and the electronics shown in Figure (3.26). The lock-in amplifier oscillator was set at 30 kHz for these measurements. A plot of the measurement data is shown in Figure (4.1).

TABLE 4.1. THEORETICAL CAPACITANCE SYSTEM STATIC CALIBRATION

ITEM	SENSITIVITIES		
	$\frac{dC}{dH}$ $\left(\frac{pF}{cm}\right)$ ±0.1	$\frac{dV}{dC}$ $\left(\frac{mV}{pF}\right)$	$\frac{dV}{dH}$ $\left(\frac{mV}{cm}\right)$ ±0.1
Theoretical Teflon TF-101	2.4		
T-13 in Graduated Cylinder (GC)(B2P23)	2.2		
T-15 in Graduated Cylinder (GC)(B2P23)	2.3		
T-15 in tank (T) (B2P108)	2.2		
Ch1 (B2P18)		3.21±0.02	
Ch2 (B2P19)		3.41±0.03	
TF-101 in Ch1			7.7
T-13 (GC) in Ch1			7.1
T-15 (GC) in Ch1			7.4
T-15 (T) in Ch1			7.1
TF-101 in Ch2			8.2
T-13 (GC) in Ch2			7.5
T-15 (GC) in Ch2			7.8
T-15 (T) in Ch2			7.5

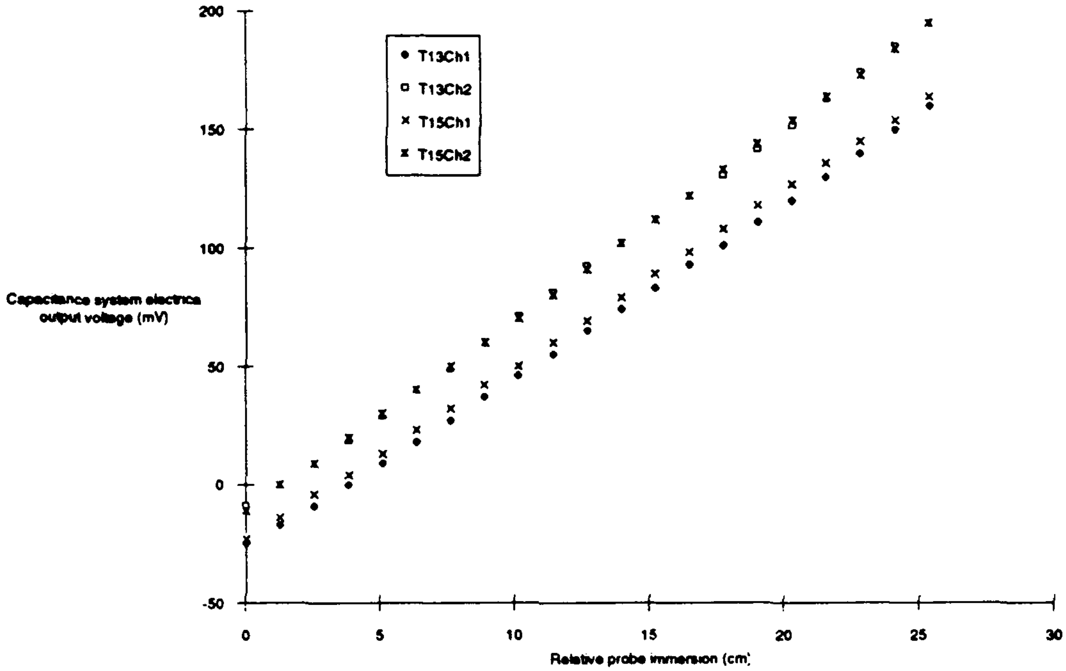

Figure 4.1. Capacitance system electrical output voltage vs. Relative immersion in the graduated cylinder (B2P24).

Capacitance system static calibrations were also conducted using the Cone Head apparatus described in Appendix B. Water was added to the Cone Head before each measurement during this test, using Omega thermocouple wire probe T-13. A plot of the measurement data is shown in Figure (4.2).

The capacitance system static voltage sensitivities for channel one measured in the graduated cylinder are in good agreement with theory. It is unknown why the capacitance system voltage sensitivities for channel two measured in the graduated cylinder were not in better agreement with theory.

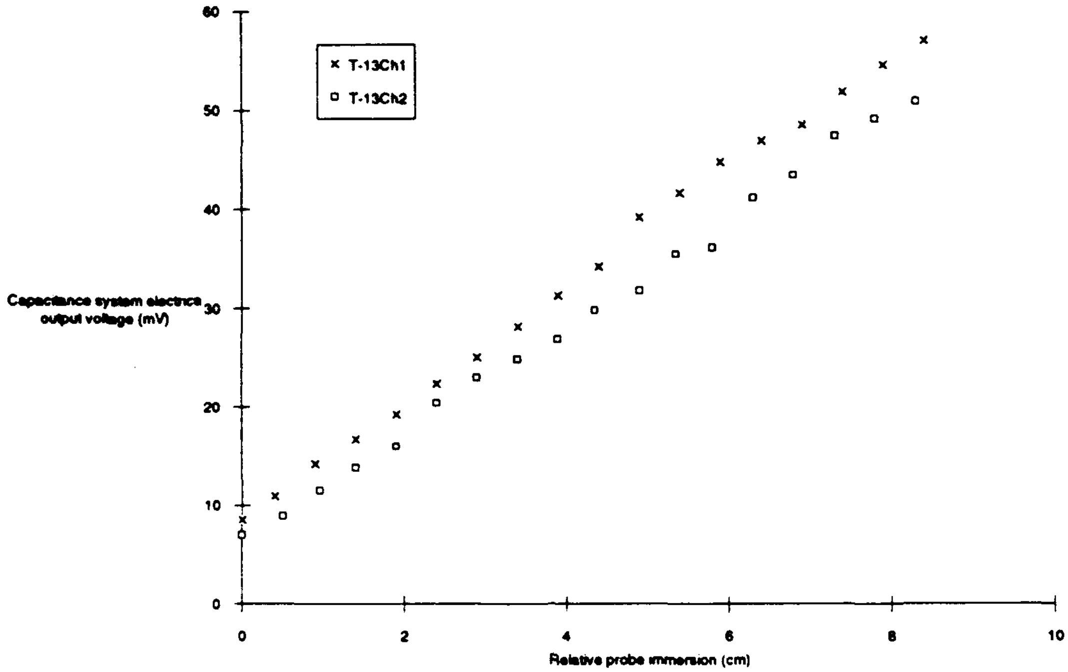

Figure 4.2. Capacitance system electrical output voltage vs. Relative immersion in the Cone Head apparatus (B3P2).

The system voltage sensitivities measured using the Cone Head apparatus are not in good agreement with theory. This is probably because of the apparatus and procedure itself. We could accurately measure the water that was being put into the Cone Head system. We could not accurately measure the amount of water that was actually getting into the changing water column. Water would stick on the sides of the graduated cylinder and the wire.

The theoretical and measured sensitivities for all the test, and the percent differences are shown in Table (4.2).

TABLE 4.2. CAPACITANCE SYSTEM STATIC SENSITIVITIES (B2P29).

System Combination	**Theoretical Sensitivity** $\frac{dV}{dH}\left(\frac{mV}{cm}\right)$ **±0.1**	**Measured Sensitivity** $\frac{dV}{dH}\left(\frac{mV}{cm}\right)$ **±0.1**	**Δ%**
T-13 & Ch1 in graduated cylinder (GC)	7.1	7.3	2.8
T-13 & Ch1 in Cone Head (CH)	7.1	6.45	-9.86
T-15 & Ch1 (GC)	7.4	7.4	0.0
T-13 & Ch2 (GC)	7.5	8.1	8.0
T-13 & Ch2 (CH)	7.5	8.5	13.33
T-15 & Ch2 (GC)	7.8	8.1	3.85

2. Conductance Static Calibrations

The properties of ordinary water are so complex that a theoretical conductance sensitivity is impractical. The important thing for these calibrations was not how do they compare with theory, but are the calibrations linear, repeatable, and measurable.

Several wire conductance static calibrations were made using the static calibration technique discussed in chapter III-C-2. One series of static measurements was made using the HP-4194A Impedance\Gain-Phase Analyzer with the

wires in either a ten gallon Pyrex beaker or the wind-wave tank. These measurements were made to compare the results from data taken in the two water samples.

The conductance sensitivity of the measurements taken in the Pyrex is 6.4 ± 0.1 mS/cm. The conductance sensitivity of the measurements taken in the wind-wave tank is 6.3 ± 0.1 mS/cm. The data from both measurements are linear, as shown in Figure (4.3).

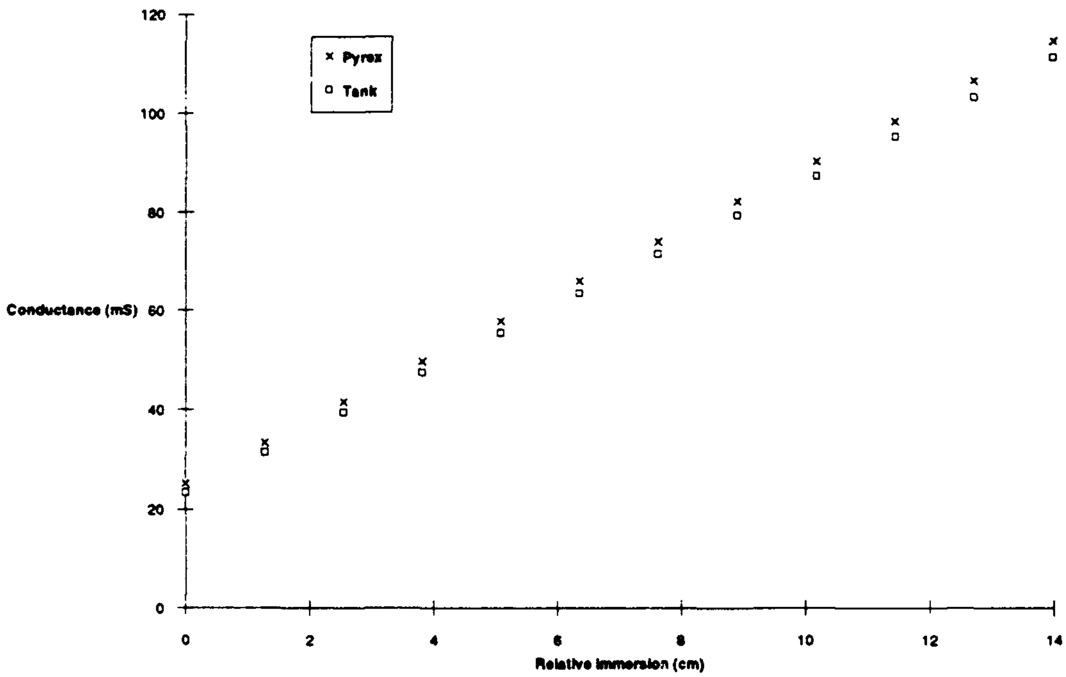

Figure 4.3. Conductance vs. Relative immersion in two water systems (B3P31).

Another series of static wire measurements were made using the same equipment, in the wind-wave tank. These measurements were made to see if two four-wire measurement combinations were possible using the five wire probe, and

how close the sensitivities were for the combinations. A gradient measurement technique was discussed, but not pursued. Table (4.3) shows the possible combinations. The wires that are used in each combination are shown filled in.

TABLE 4.3. FOUR WIRE COMBINATIONS WITHIN THE FIVE WIRE PROBE (B3P39).

Four Wire Combination Number	**Four Wire Combinations**
SU1	●●●●⊙
SU2	●●●⊙●
SU3	⊙●●●●
SU4	●⊙●●●

We used deviations in the conductance measurements to ensure that all the individual wires were straight as possible. We did use the tensioning loops to adjust some of the wires. The final measured conductance sensitivity and deviation results are shown in Figures (4.4 and 4.5).

The conductance sensitivities, shown in Table (4.4), of the various four-wire combinations are different because of the two different probe geometries, four in a row or a space inserted. These geometries put the voltage probes in different potential fields between the current probes. The SU1 and SU3 configurations have lower sensitivities than the SU2 and SU4 configurations because the ΔV is the lowest in

this symetric configuration. The highest sensitivity should be obtained when the center probe is not used.

The conductance sensitivity measurements were linear, with high correlation coefficients, and the deviations were consistent for all the combinations with a maximum error of 0.4%. The causes of the anomalies of the last data points for SU1 and SU4 are unknown. We choose to use wire combinations SU2 and SU4 in all latter test because they had the highest conductance sensitivities, as expected.

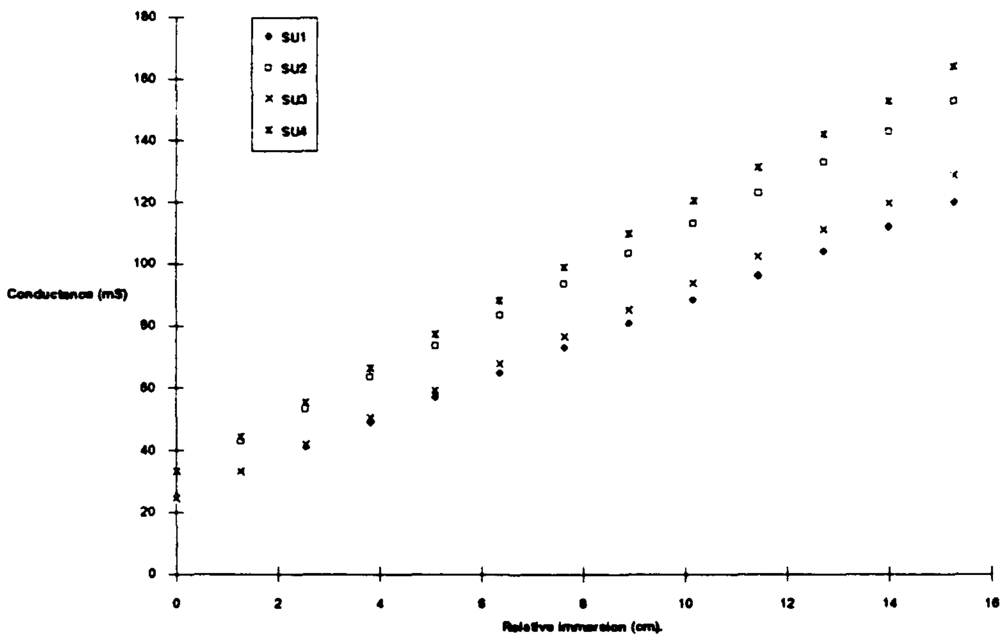

Figure 4.4. Conductance vs. Relative immersion for various four wire combinations (B3P42).

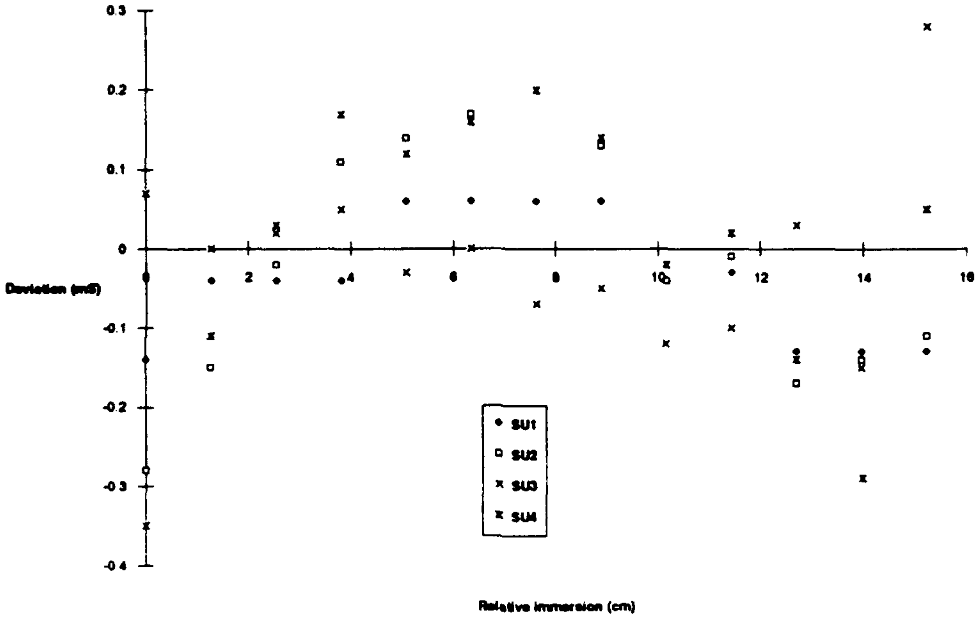

Figure 4.5. Deviation vs. Relative immersion for various four wire combinations (B2P42).

TABLE 4.4. FOUR WIRE CONDUCTANCE SENSITIVITIES (B3P42).

Four Wire Combination Number	**Conductance Sensitivity** $\frac{mS}{cm}$ **(±0.1)**
SU1	6.2
SU2	7.9
SU3	6.8
SU4	8.6

Conductance system static calibrations were made to determine the voltage sensitivities which would become inputs for the engineering units of the HP-3562A Dynamic

Analyzer power spectrum measurements. The lock-in amplifiers provided electrical inputs to the conductance electronics. The conductance electronics electrical output was then measured using two hand held multimeters, one for each channel.

The voltage sensitivity for channel one is 0.309 ± 0.005 V/cm, and for channel two is 0.381 ± 0.005 V/cm. The data from the measurements was linear, as shown in Figure (4.6).

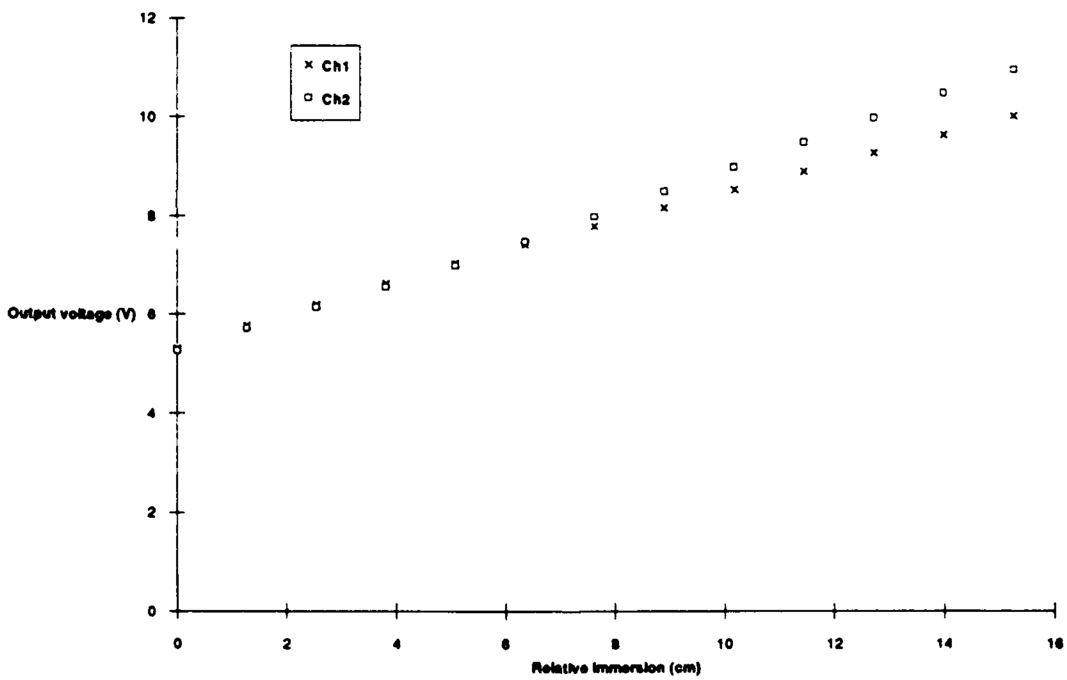

Figure 4.6. Output voltage vs. Relative immersion for conductance system electronics (B3P59).

B. DYNAMIC CALIBRATIONS

1. Capacitance Dynamic Calibrations

Several capacitance dynamic calibration apparatus and techniques were tried, as described in Appendix B. The apparatus was cumbersome, and the results of the techniques were not repeatable. The repeatability problem was caused by the low tank impedance, the results of this test were described in the previous chapter.

It was also determined that all the capacitance dynamic calibration techniques were not conducted in the preferred motion either. These techniques moved the wire up and down in the water. This does not represent a traveling gravity wave motion.

The *low, approximately 20 ohm,* tank impedance made a two wire capacitance system unusable when combined with the unknown and unstable water properties. Unfortunately, the tank impedance test was not conducted until late in the capacitance data collection efforts.

2. Conductance Dynamic Calibrations

Conductance dynamic calibrations were conducted to determine repeatability, if there was a preferred probe orientation, and to determine the frequency response. The calibrations were conducted in the small wave guide to cut off low frequency parametric waves, using the techniques described in chapter III-C-3.

Four consecutive measurements were taken in the same location, with three different probe orientations. The line of wires in the probe were either normal or parallel to the paddle. The first measurement of the sequence was always parallel to the paddle. Two measurements were always made with the wires parallel to the paddle.

The two parallel measurements were the test of repeatability. The other measurements were the test for best probe orientation. The probe frequency response could be determined at all orientations.

A two Hertz, one to four Hertz, dynamic power spectrum calibration was conducted in the small wave guide. Waves below two Hertz were not sinusoidal on the oscilloscope, which set the lower frequency limit. The Flat Top window was used for these measurements because this window has the lowest equipment, HP-3562A Dynamic Analyzer, amplitude accuracy uncertainty of up to ± 0.1 dB [Ref. 35].

The engineering units used in the HP-3562A internal power spectrum calculations were determined from the results of the static calibrations discussed in section A(2).

The parallel probe orientation consistently had the highest sensitivity at any given frequency for both channels, as shown in Figure (4.7 and 4.8). The data point at four Hertz is above the parametric wave cutoff for the small guide. The last data points show a definite interaction between the gravity and parametric waves for all

probe orientations. The parallel probe orientation was also very repeatable, except for the anomaly at the 2.5 Hertz knee.

The HP-3562A Dynamic Analyzer measurements were verified by measuring wave peak-to-peak amplitudes using a HP-54501A Digitizing Oscilloscope. The amplitudes ranged from 330 mV at two Hertz to 187 mV at four Hertz (B3P68-90).

The very disappointing result was that the probe frequency response was not flat, not even for an octave. We have assumed that the probe response would continue to drop with frequency, but could not test the higher frequencies because of the parametric waves caused by the paddle. The current probe construction would not allow for a smaller wave guide, which would enable us to test at higher frequencies.

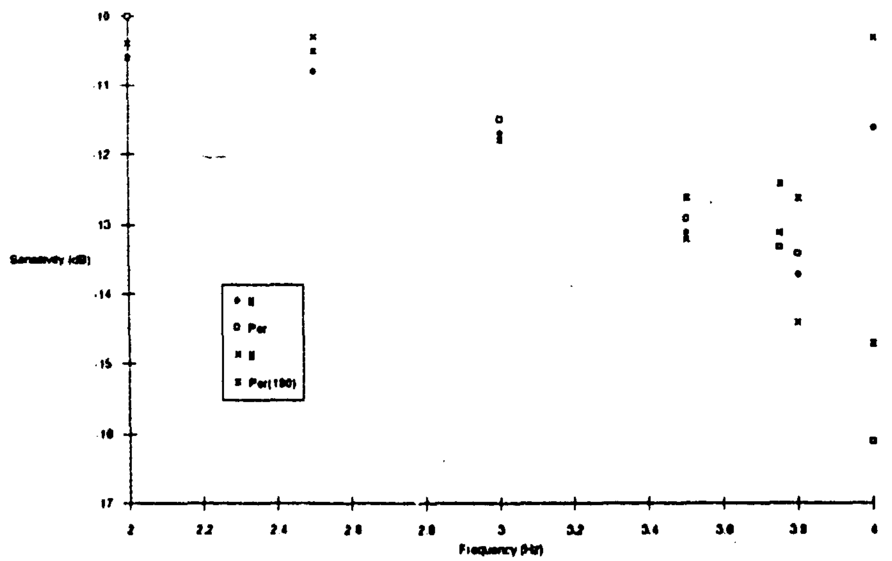

Figure 4.7. Sensitivity vs. Frequency for channel one (B3P64-67).

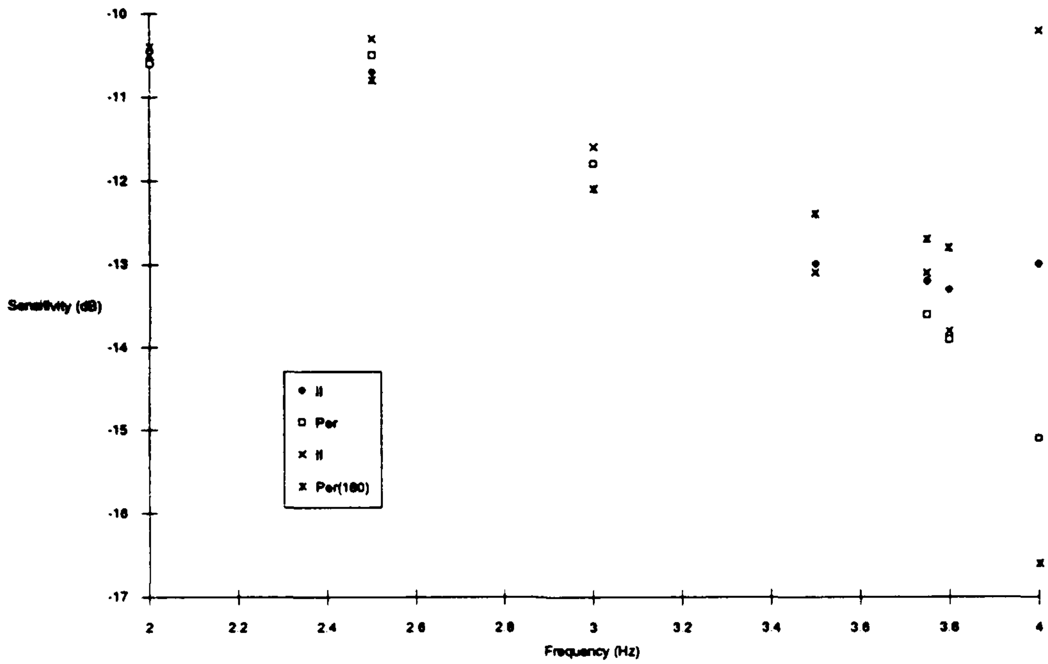

Figure 4.8. Sensitivity vs. Frequency for channel two (B3P64-67).

C. TANK MEASUREMENTS

Measurements were taken in the wind-wave tank throughout the experiment. The sensor may or may not have been statically calibrated prior to any particular measurement. No tank measurements were made after the conductance system dynamic calibrations were made.

Results of early phase speed and power spectrum capacitance system measurements were presented at the 119th meeting of the Acoustical Society of America, at Penn State University [Ref. 36].

The cross correlation plot in Figure [4.9] is a typical capacitance system measurement phase speed plot. The data

were analyzed using the least square fit technique. This 1.35 ± 0.01 Hertz, driven gravity wave has a measured frequency of 1.36 ± 0.01 Hertz. The measured delay time is 15.6 ± 0.1 msec. The probes had a measured separation of 0.025 ± 0.01 m.

The theoretical phase speed for this driven gravity wave, using equation [2.3], is 1.16 ± 0.01 m/sec. The measured phase speed, using equation [2.25], is 1.63 ± 0.01 m/sec. This is a 40.7% difference. It is possible that electrical cross-talk between the two channels in the electronics box may have decreased the delay time measured.

The theoretical wavelength for this same wave, using equation [2.26], is 0.86 ± 0.01 m. The measured wavelength is 1.20 ± 0.01 m. This is a 39.9% difference.

The capacitance system equipment and techniques were both adjusted, and the measured phase speed and wavelength were consistently higher than theory. We believe the results are high due to an erroneous delay time in the channel two output caused by electrical cross-talk in the electronics box, but this was not confirmed.

Base line noise and wind power spectrum measurement plots, using a statically calibrated capacitance system, are shown in Figure (4.10). Similar data obtained with the conductance system is shown in Figure (4.11). The four upper lines in Figure (4.10) are wind power spectrums, at four different wind speeds. Spectra for both the capacitance and

conductance systems peak at approximately two Hertz and decay at approximately 50 to 70 dB per decade, or with power decaying at ω^{-5} to ω^{-7}, but the slope of the decay may not be trustworthy because the transducer was not dynamically calibrated and its frequency response is unknown. However, there is excellent agreement in the wind power spectrum measurements for the two transduction systems.

S-17 1.35 Hz T11-T12

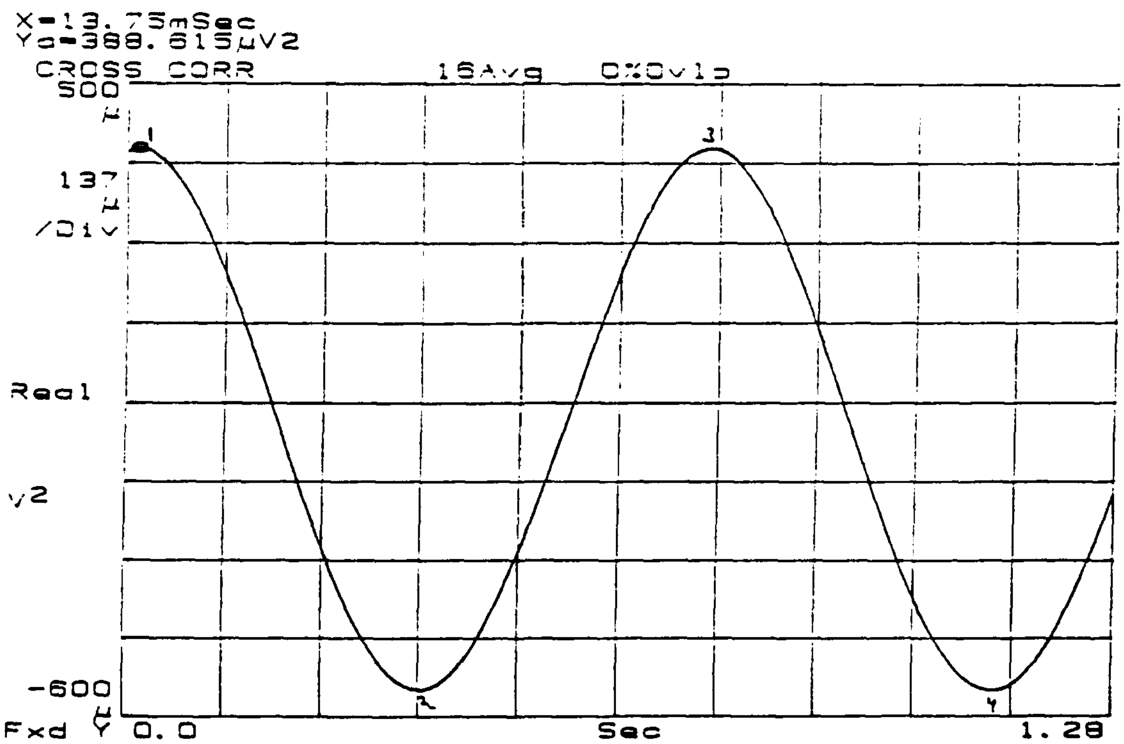

1- 16.25 mSEC
2- 383.75 mSEC
3- 752.5 mSEC
4- 1.1225 SEC

Y ± 0.001 = 0.0156 ± 0.0007 + 0.3688 ± 0.0004
r = 0.9999989

Figure 4.9. Capacitance system cross correlation plot.

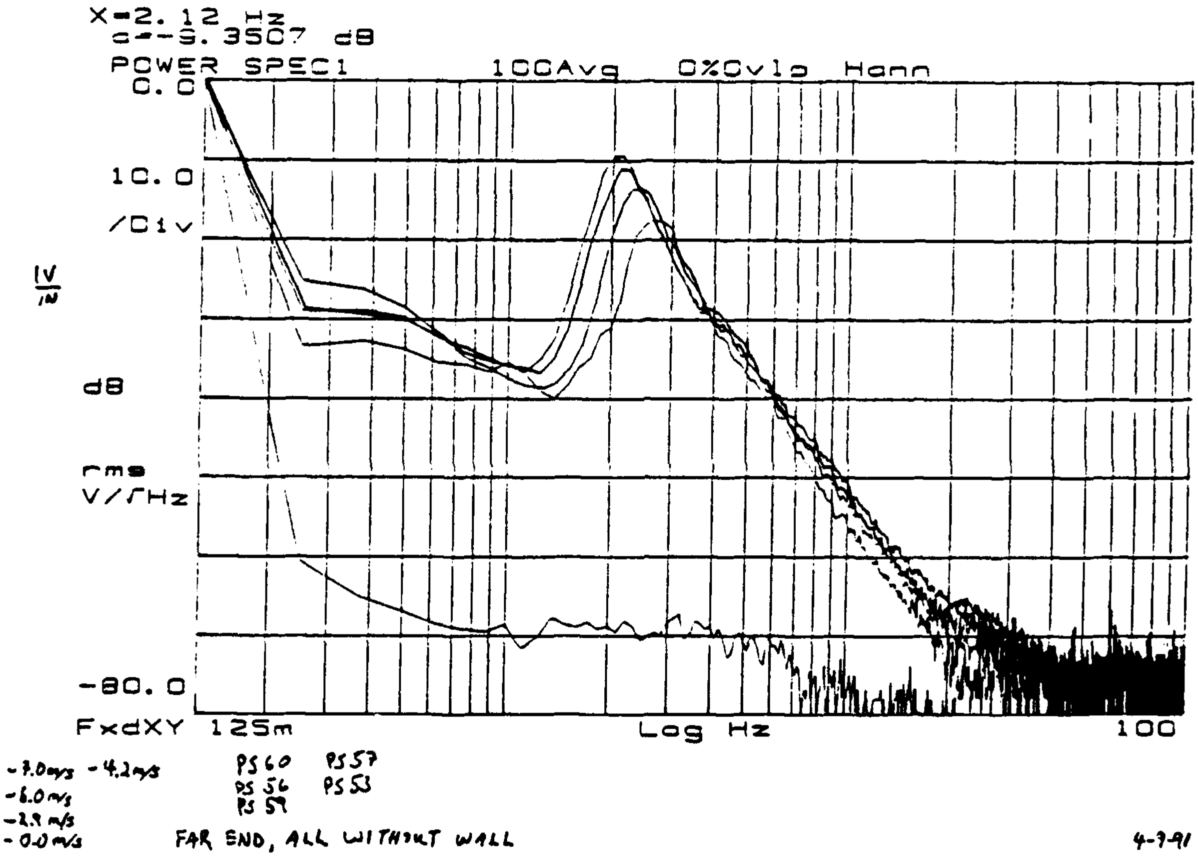

Figure 4.10. Capacitance system base line noise and wind power spectra plot.

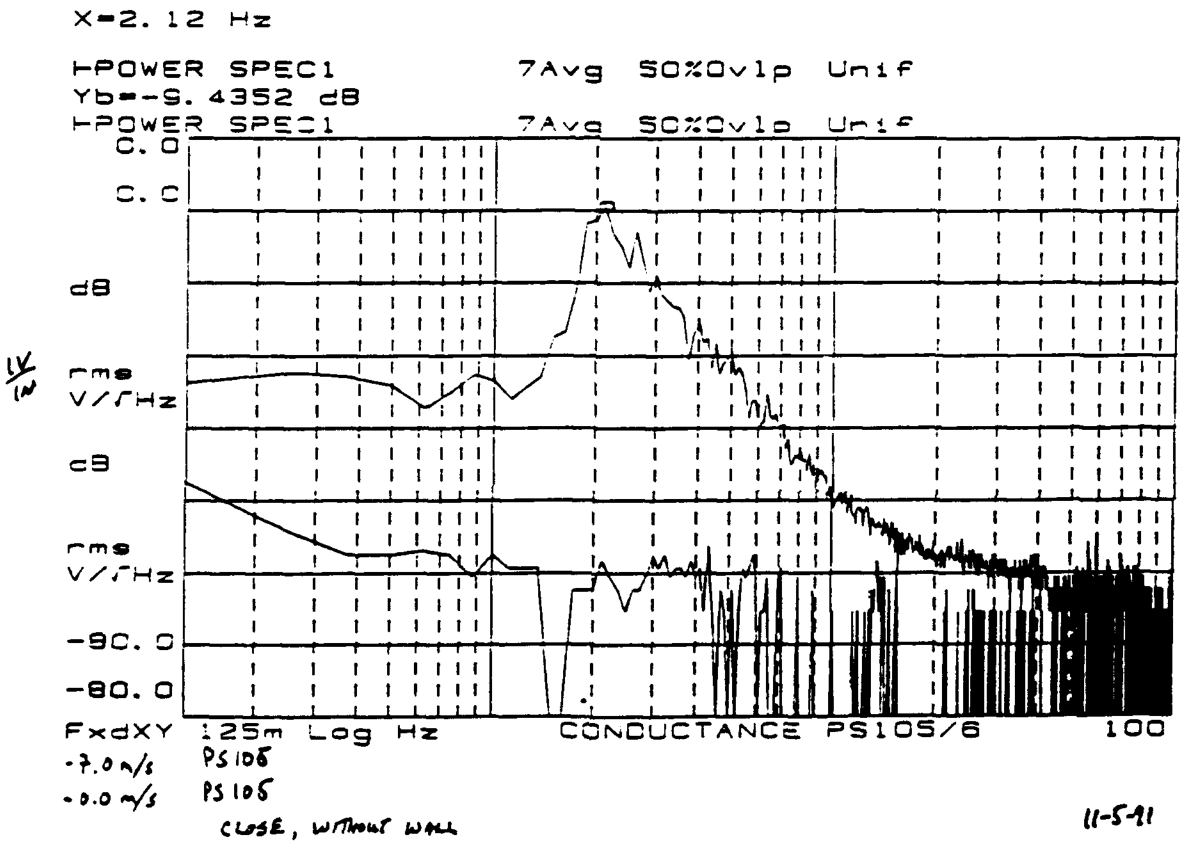

Figure 4.11. Conductance system base line noise and wind power spectra plot.

Power spectra of (a) Base line noise, (b) driven gravity wave, and (c) driven gravity wave with wind, using a statically calibrated capacitance system, are shown in Figure (4.12). The driven gravity wave spectrum shows the harmonics of the driving frequency, at least 18 dB below the fundamental. There is very little energy above the noise level at other frequencies.

The driven gravity wave and wind spectrum is approximately 20 dB above the noise and the driven gravity wave spectrum. The wind energy completely dominates the harmonics of the driven gravity wave with this particular frequency resolution. The wind decay is unaffected by the addition of the driven gravity wave. The decay of the power is approximately as ω^{-6}.

The power spectra plots of the driven gravity wave and driven gravity wave with wind were expanded to 0.5 Hz about the fundamental driven frequency, shown in Figure (4.13). The energy peak is downshifted 0.062 Hz when wind is added. A second, lower frequency energy peak is also observed. This peak is approximately 30 dB above the noise level. This peak may be caused by the non-linear effects discussed in Dr. Larraza's theory. Determining the cause(s) of the additional energy peak and the fundamental frequency downshifting were left for follow-on theses.

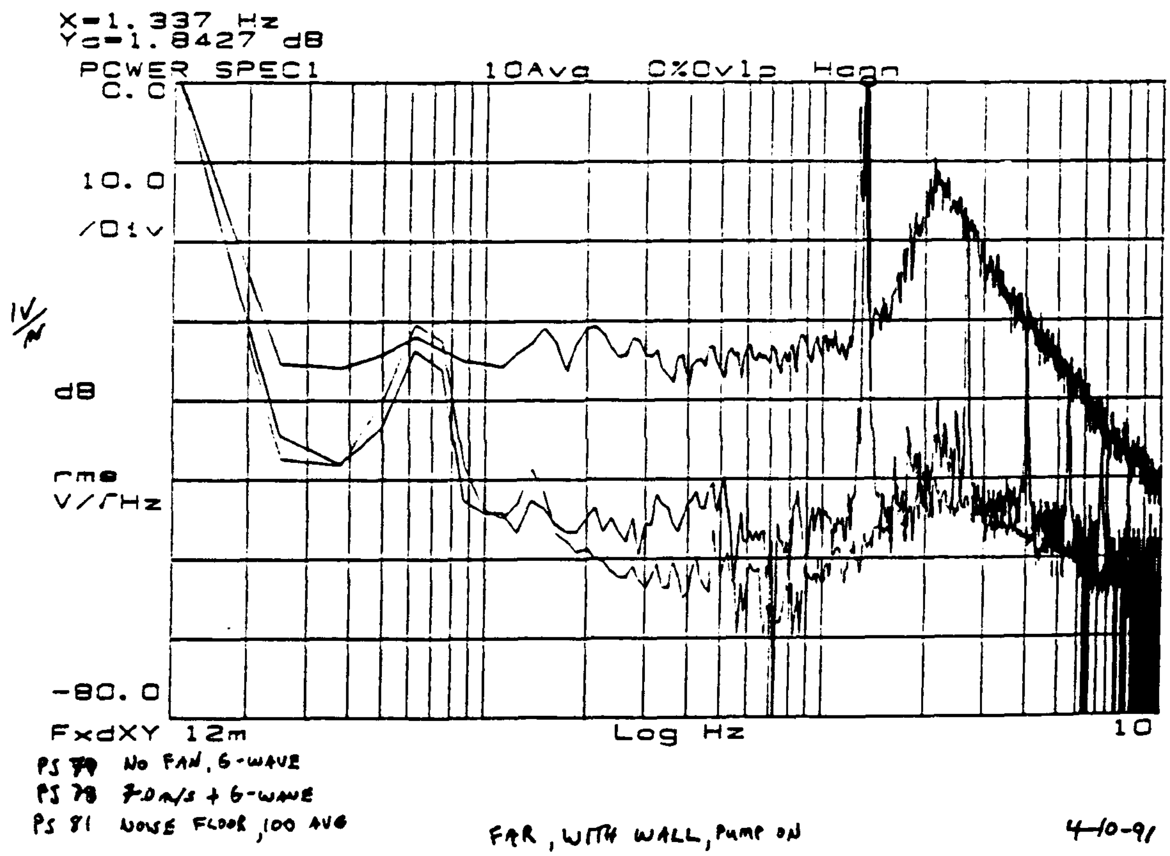

Figure 4.12. Capacitance system base line noise, driven gravity wave, and driven gravity wave with wind power spectra plot.

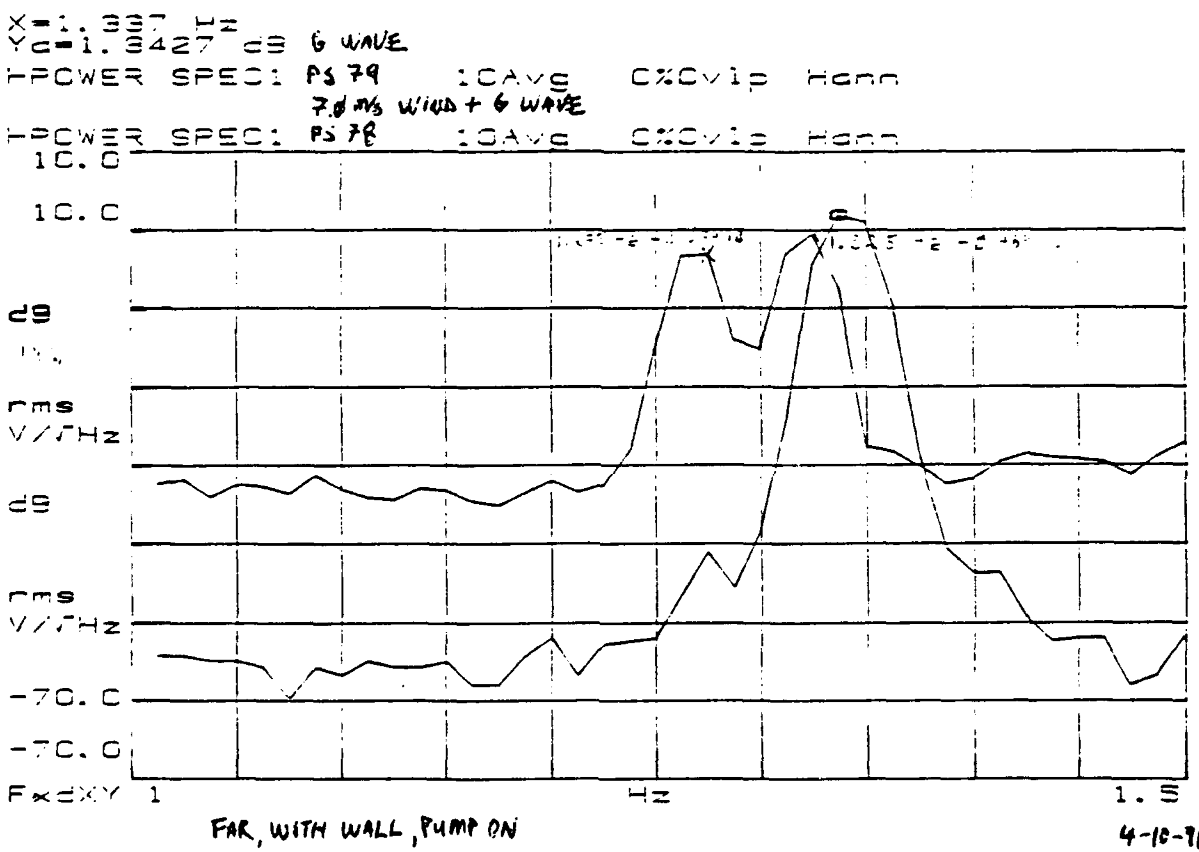

Figure 4.13. Expanded plot of driven gravity wave and driven gravity wave with wind.

Plots of the tank quality factor measured with the capacitance system, are shown in Figure (4.14) and similar data obtained with the conductance system is shown in Figure (4.15). The tank Q measurement with the conductance system was almost double the capacitance system measurement's value at the low frequencies, and half the value at the higher frequencies. It is unknown why and how there is a difference in tank Q for the two measurement techniques. The measured Q at different frequencies is shown in Figure (4.16).

The driven gravity wave spectrum was not measured using the conductance system. All efforts were directed at getting a dynamic calibration for the conductance system instead. We were not sure of the best method to make phase speed and wavelength measurements with the conductance probe at that time.

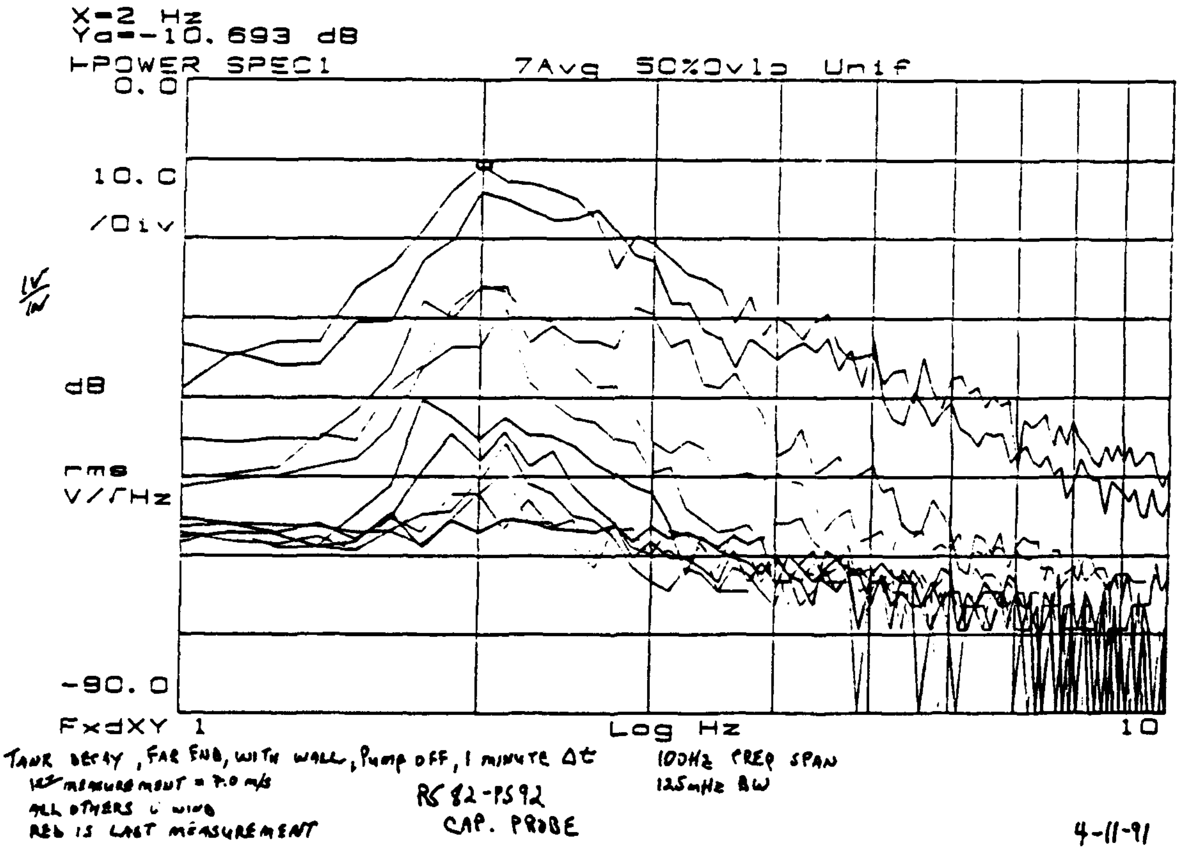

Figure 4.14. Tank Q capacitance system measurement plot.

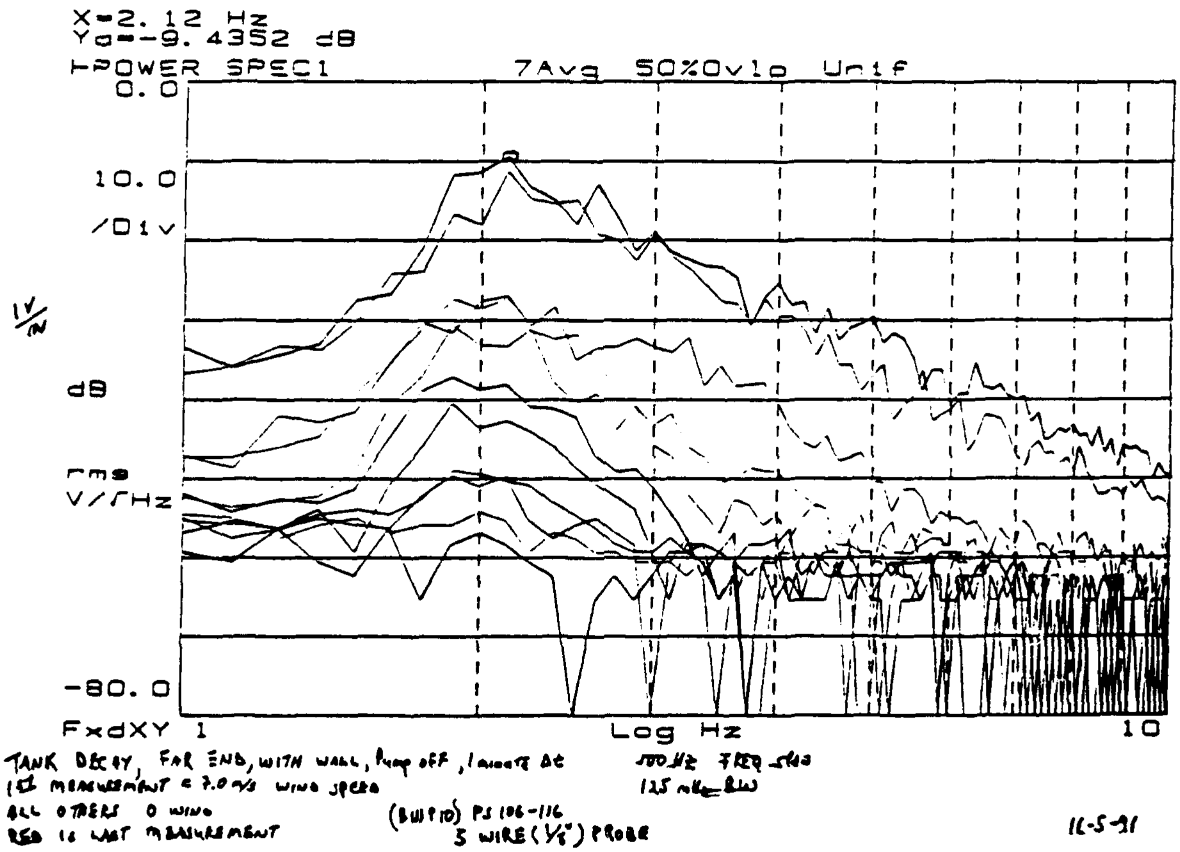

Figure 4.15. Tank Q conductance system measurement plot.

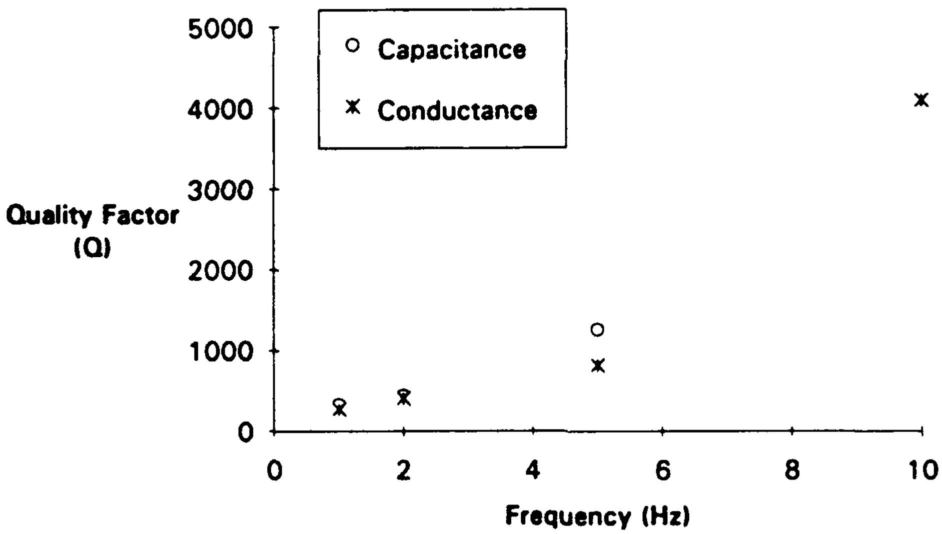

Figure 4.16. Tank quality factor vs. Frequency measured by capacitance and conductance systems (B2P137-142 and B3P10).

V. CONCLUSIONS

Capacitance and conductance measurements using two and four wire techniques were developed, tested, and calibrated in this thesis. The four wire conductance system technique was determined to be the better of the two tested, and is currently being used in a follow on thesis. The two wire capacitance system repeatability problems caused by grounding and the complex properties of "simple" water are not present using the four wire technique. The two systems did give quite similar results for wind-wave spectra.

We feel the four-wire technique is superior to the two-wire technique as long as the potential problems in conducting a water surface wave height measurement, dirty probes and unknown variable water chemistry, only exist on a microscopic scale. This thesis did not prove or set limits to this assumption. A study of these problems is suitable and desirable as a follow on thesis.

Static calibrations were performed many times on all systems. The results of the various tests were consistent, linear, and generally compared well with theory. The static calibration techniques are simple and should be completed prior to other measurements in future experiments.

The results of the conductance system dynamic calibration were disappointing and puzzling because the frequency response was not flat. It is difficult to infer

what the frequency response is in the entire frequency range of interest, 0-10 Hz, due to the limited results we were able to obtain. However, the two systems gave quite silimar results for the wind-wave spectra.

Driven gravity wave frequency downshifting and wind energy dumping was observed in the combined gravity wave and wind-wave measurements. A follow-on thesis will explore this.

The importance of the dynamic calibration is unknown for future nonlinear experiments and should be reviewed to insure that important data is available and interpretations are accurate.

The most important thing I learned from this research are some basic principles of experimental science. First, you must have some idea concerning what and why you are investigating nature. Second, you must have a predetermined purpose and procedure for the investigation. Third, data must be recorded thoroughly, meticulously, and in a timely manner. Fourth, you must evaluate the data carefully to determine the outcome of your experiment. Finally, you need **GOOD LUCK**.

APPENDIX A

I. HP-15C CALCULATOR LEAST SQUARES FIT STANDARD DEVIATIONS PROGRAM CODE

The standard deviations in all the least squares fit parameters were discussed in chapter II E. This is program code for the HP-15C hand held calculator, which can be used to solve equations (2.16 through 2.19) for data entered into the calculator using the summation key (B1P66/67). The calculator stores the different summation values in the following register as shown in Table (A.1).

TABLE A.1. HP-15C REGISTER VALUES AFTER USING SUMMATION KEY.

Register	Value
2	N, the number of samples
3	summation of x_n
4	summation of x_n^2
5	summation of y_n
6	summation of y_n^2
7	summation of $x_n y_n$

The standard deviations in y, slope, and intercept are displayed at program lines 040, 054, and 067 respectfully. The program code is shown below.

Program function	Program line number	Calculator keys
g[P/R]	000	
f[LBL]C	001	42,21,13
RCL[5]	002	45,5
g[x^2]	003	43,11
RCL[4]	004	45,4
x	005	20
2	006	2
ENTER	007	36
RCL[7]	008	45,7
x	009	20
RCL[3]	010	45,3
x	011	20
RCL[5]	012	45,5
x	013	20
CHS	014	16
-	015	30
RCL[2]	016	45,2
ENTER	017	36
RCL[7]	018	45,7
g[x^2]	019	43,11
x	020	20
+	021	40
RCL[2]	022	45.2
ENTER	023	36
RCL[4]	024	45,4
x	025	20
RCL[3]	026	45,3
g[x^2]	027	43,11
-	028	30
÷	029	10
CHS	030	16
RCL[6]	031	45,6
+	032	40
RCL[2]	033	45,2
ENTER	034	36
2	035	2
-	036	30
÷	037	10
$\sqrt{x}$	038	11
STO[8]	039	44,8
R/S	040	31
RCL[4]	041	45,4
ENTER	042	36
RCL[4]	043	45,4
ENTER	044	36
RCL[2]	045	45,2
x	046	20

RCL[3]	047	45,3
g[x^2]	048	43,11
-	049	30
÷	050	10
$\sqrt{x}$	051	11
RCL[8]	052	45,8
x	053	20
R/S	054	31
RCL[2]	055	45,2
ENTER	056	36
RCL[2]	057	45,2
ENTER	058	36
RCL[4]	059	45,4
x	060	20
RCL[3]	061	45,3
g[x^2]	062	43,11
-	063	30
÷	064	10
$\sqrt{x}$	065	11
RCL[8]	066	45,8
x	067	20
g[RTN]	068	43,32

APPENDIX B

I. CAPACITANCE SYSTEM DYNAMIC CALIBRATIONS

This section will briefly describe the equipment and techniques used for the capacitance system dynamic calibrations. Two dynamic calibrations of the capacitance system were explored before the capacitance system was determined to be unusable. Both of the techniques moved the water or the sensor probe, up and down, which we decided was not the preferred motion for the dynamic calibration.

A. Cone Head

A 16 ounce plastic funnel, or cone, was used to connect a 110 ml glass burette to a USRD Type J-11 Transducer, hence the Cone Head name for the apparatus. The J-11 provided a means to convert an electrical signal to fluid motion and the funnel acted as a fluid amplifier with a gain of approximately 130. All capacitance system measurements were actually made in the burette.

The top of the probe wire was held in place at the top of the burette with a small cork stopper. Fishing line was tied to the bottom of the capacitance probe. The fishing line was passed around a large paper clip lodged in the funnel, pulled out of the top of the burette to tension the probe wire and held in place at the top of the burette with the same small cork stopper.

All joints in the Cone Head were sealed for water tight integrity with Polymeric Systems, Inc., PSI 601 Clear, 100% Silicone, RTV Adhesive Sealant. The Cone Head apparatus is shown in Figure (B.1).

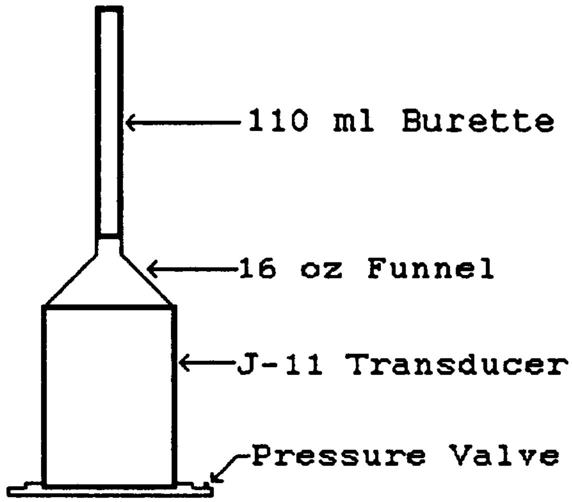

Figure B.1. Cone Head apparatus.

The J-11 transducer motion was calibrated using an LVDT. The J-11 compensation bladder pressure was measured using a PX-126, Omega Engineering, Inc. differential pressure transducer. This provided a non-intrusive measurement of the J-11 when the Cone Head was assembled.

The electrical outputs of the LVDT and pressure transducer were compared when a low frequency square wave was applied to the J-11. The Cone Head was assembled with water in the apparatus and the electrical output of the pressure transducer was then compared with the capacitance system output.

This calibration scheme was not refined due to the fact that only one sensor probe could be fit into the Cone Head at a time and the poor results in the Cone Head static calibrations.

B. Motor

This technique was briefly tested, with no documented results. The sensor probe was moved up and down in the wind-wave tank, while the probe was on the Harp.

A 1/4 horsepower AC motor was bolted to the top U channel on the Harp. A 2.5 inch diameter pulley was mounted eccentrically to the motor shaft. A one inch diameter pulley was mounted directly above the probe. One end of an approximately 24 inch long, ten pound, fishing line was tied to the top of the probe, placed in the grooved flywheel, and the other end of the fishing line was tied to a standoff post on the 2.5 inch pulley. The other end of the probe was connected to the lower U channel with two number one rubber bands.

The AC motor was plugged into a variable transformer which would adjust the mechanical output frequency of the large flywheel and provide the forcing function for the probe.

APPENDIX C

I. HP-3562A DYNAMIC SIGNAL ANALYZER FRONT PANEL CONTROL SEQUENCE TO STORE DATA ON DISK

The front panel hard disk accessing sequence for the HP-3562A Dynamic Signal Analyzer using the HP-9133 Disk Drive is shown in Table (C.1). Complete operating instructions can be found in Reference 35.

TABLE C.1. HP-3562A HARD DISK ACCESSING SEQUENCE.

Step	Menu	Select
1	HP-IP FCTN	Select Address
2	SELECT ADDRESS	Disc Address = 0 Disc Unit = 1
3	DISC	Save/Recall File

LIST OF REFERENCES

1. Gleick, J., *Chaos, Making a New Science*, Penguin Books, 1988.

2. Phillips, O. M., "The equilibrium range in the spectrum of wind-generated waves," *J. Fluid Mech.*, v.4, pp. 426-434,1958.

3. Zakharov, V. E. and Filonenko, N. N. "Energy Spectrum For Stochastic Oscillations Of The Surface Of A Liquid," *Soviet Phys. Dokl.*, v.11, pp. 881-883, 1965.

4. Larraza, A., *Universal Power Spectra for Wave Turbulence: Applications to Wind Waves, Flicker Noise, Solar Wind Spectrum, and Classical Second Sound*, Ph.D. Dissertation, University of California at Los Angeles, Los Angeles, California, August 1987.

5. Donelan, M. A., Hamilton, J., and Hui, W. H., "Directional Spectra Of Wind-Generated Waves," *Phil. Trans. R. Soc. Lond. A*, v. 315, pp. 509-562, 1985.

6. Ramamonjiarisoa, A. and Coantic, M.,"MECANIQUE DES FLUIDES-Loi experimentale de dispersion des vagues produites par le vent sur une faible longueur d' action," *Acedemie Des Sciences, Paris, Comptes Rendus, Series B: Sciences Physiques*, v. 282, pp.111-114, 1976.

7. Rikiishi, K., "A New Method for Measuring the Directional Wave Spectrum. Part I. Description," *J. Phys. Oceanography*, v. 8, pp. 508-517, 1978.

8. Rikiishi, K., "A New Method for Measuring the Directional Wave Spectrum. Part II. Measurement of the Directional Spectrum and Phase Velocity of Laboratory Wind Waves," *J. Phys. Oceanography*, v. 8, pp. 518-529, 1978.

9. Larraza, A. and Garrett, S. L., "Wave Turbulence and the Search for Classical Second Sound," Naval Postgraduate School Preliminary Proposal for Research, 10 January 1989.

10. Larraza, A., Garrett, S. L., and Putterman, S., "Dispersion relations for gravity waves in a deep fluid: Second sound in a stormy sea," *Physical Review A*, v. 41, No. 6, pp. 3144-3155, 15 March 1990.

11. Lighthill, M. J. Sir, *Waves in Fluids*, p. 210, Cambridge University Press, 1978.

12. Landau, L.D. and Lifshitz, E.M., *Fluid Mechanics, vol. 6 of Course of Theoretical Physics*, pp. 36-37, Pergamon Press, 1959.

13. Lighthill, M. J. Sir, *Waves in Fluids*, pp. 204-214, Cambridge University Press, 1978.

14. Landau, L.D. and Lifshitz, E.M., *Fluid Mechanics, vol. 6 of Course of Theoretical Physics*, pp. 1-39, Pergamon Press, 1959.

15. Ibid, p. 3.

16. Halliday, D. and Resnick, R., *Fundamentals of Physics*, 2d ed., p.487, John Wiley & Sons, Inc., 1970.

17. *HP-4192A LF Impendance Analyzer Operation and Service Manual*, PN 04192-90001, p. 3-48, Hewlett-Packard, 1984.

18. Taylor, J. R., *An Introduction to Error Analysis, The Study of Uncertainties in Physical Measurements*, pp. 153-168, University Science Books, 1982.

19. Ibid, p. 176.

20. Taylor, J. R., *An Introduction to Error Analysis, The Study of Uncertainties in Physical Measurements*, pp. 182-184, University Science Books, 1982.

21. Ibid, p. 249.

22. Ibid, pp. 81-87.

23. *The Fundamentals of Signal Analysis Application Note 243*, p. 46, Hewlett-Packard, 1985.

24. Ibid, p. 55.

25. Ibid, p. 54.

26. Kinsler, L. E., Frey, A. R., Coppens, A. B., Sanders, J. V., *Fundamentals of Acoustics*, 3rd ed., p.9, John Wiley & Sons, Inc., 1982.

27. Ibid, p.16.

28. Ibid, pp.7-16.

29. Medwin, H. and Clay, C. S., "Dependance of Spatial and Temporal Correlation of Forward-Scattered Underwater Sound on the Surface Statistics. II Experiment," *J. Acoustical Society of America*, v. 47 no.5 (part 2), pp. 1419-1429, 1970

30. Zero-max®, Instruction and Parts Booklet IPB-282, *Instruction and parts booklet for zero-max drives, motors a d gearheads*, 1982.

31. DuPont, Technical Bulletin T-4A, *Teflon FEP*, p. 3, December 1986.

32. Burr-Brown, *Burr-Brown integrated circuits data book*, vol. 33, pp. 2-55 through 2-65, Burr-Brown Corporation, 1989.

33. Abramowitz, M. and Stegun, I. E., *National Bureau of Standards Applied Mathematics Series, Handbook of Mathematical Functions with Formaulas, Graphs, and Mathematical Tables*, number 55, pp. 870-873, U.S. Department of Commerce, December 1972.

34. Analog Devices, Inc., *1988 Linear Products Databook*, pp. 6-13 through 6-21, Analog Devices, Inc., 1988.

35. Hewlett-Packard Company, *HP3562A Operating Manual*, HP-03562-90001, Hewlett-Packard Company, 1988.

36. Larraza, A., Yarber, R. K., and Garrett, S. L., "An experimental search for calssical sound in a system of nonlinear random waves," presented at the 119th meeting of the Acoustical Society of America, Penn State University, State College, Pennsylvania, 21-25 May 1990, J. Acoustical Society of America, Supp. 1 **87**, S55, Spring 1990.

DISTRIBUTION LIST

1.	Dr. Michael F. Shlesinger Office of Naval Research Code 1112 800 N. Quincy St. Arlington, VA 22217-5000	1
2.	Library, Code 52 Naval Postgraduate School Monterey, CA 93943-5002	2
3.	Physics Department, Code PH Naval Postgraduate School Monterey, CA 93943-5000	1
4.	Physics Department, Code PH/Kn Naval Postgraduate School Monterey, CA 93943-5000	2
5.	Physics Department, Code PH/Gx Naval Postgraduate School Monterey, CA 93943-5000	2
6.	Physics Department, Code PH/Yb Naval Postgraduate School Monterey, CA 93943-5000	3
7.	Physics Department, Code PH/Mr Naval Postgraduate School Monterey, CA 93943-5000	1
8.	Dr. Charles L. Burmaster MITRE Corporation Navy Systems and Technology Division Washingtion C^3 Center Mc Lean, VA 22101-3481	1
9.	Defense Technical Information Center Cameron Station Alexandria, VA 22304-6145	2